Contents lists available at SciOpen

Food Science and Human Wellness

journal homepage: https://www.sciopen.com/journal/2097-0765

China Food Publishing Co.

Comparative analysis of *Andrias davidianus* bone-derived peptides from distinct habitats and their antihyperuricemic activity

Wei Li[a,1], Hongliang Chen[a,1], Haihong Chen[a], Bing Xu[a,c], Xinhui Xing[a,b,c,d,e,*]

[a] *Institute of Biopharmaceutical and Health Engineering, Tsinghua Shenzhen International Graduate School, Shenzhen 518055, China*
[b] *Key Laboratory of Active Proteins and Peptides Green Biomanufacturing of Guangdong Higher Education Institutes, Tsinghua Shenzhen International Graduate School, Shenzhen 518055, China*
[c] *Institute of Biomedical Health Technology and Engineering, Shenzhen Bay Laboratory, Shenzhen 440300, China*
[d] *Key Laboratory for Industrial Biocatalysis, Ministry of Education, Institute of Biochemical Engineering, Department of Chemical Engineering, Beijing 100084, China*
[e] *Center for Synthetic and Systems Biology, Tsinghua University, Beijing 100084, China*

ARTICLE INFO

Article history:
Received 7 August 2025
Received in revised form 7 September 2025
Accepted 9 October 2025

Keywords:
Andrias davidianus bone
Peptides
Composition analysis
High performance liquid chromatography fingerprint
Antihyperuricemic activity

ABSTRACT

Andrias davidianus bone peptides (ADBP), known for their potent xanthine oxidase (XOD) inhibitory activity, show promise as adjunctive agents for the treatment of hyperuricemia (HUA). However, their quality control and antihyperuricemic efficacy across different farming regions have not been thoroughly investigated. This study undertook a comparative analysis of ADBP from nine representative farming locations, developed a high-performance liquid chromatography (HPLC) fingerprint, and evaluated the antihyperuricemic activity of the most promising sample both *in vitro* and *in vivo*. The nine ADBP samples predominantly consisted of low-molecular-weight peptides with high protein content. However, their mineral and amino acid profiles exhibited significant variability, which served as key distinguishing markers. A reliable HPLC fingerprint was established to characterize ADBP from the different farming regions. Based on compositional analysis and XOD inhibitory activity, the ADBP obtained from the Hunan Zhangjiajie (HNZJJ) region was selected for further investigation. *In vitro* experiments utilizing an optimized adenosine-induced HUA model in LO_2 cells confirmed the uric acid-lowering effect of the selected ADBP. *In vivo* experiments using a mouse model demonstrated that ADBP significantly suppressed hepatic uric acid synthesis by inhibiting adenylate deaminase (ADA), XOD activity, and reducing serum uric acid levels. Additionally, ADBP alleviated HUA-induced liver damage by enhancing hepatic antioxidant defenses. Metabolomic analysis revealed that ADBP-induced alterations in liver metabolites may contribute to the alleviation of HUA. These metabolites were notably enriched in pathways related to linoleic acid metabolism, arginine and proline metabolism, caffeine metabolism, cysteine and methionine metabolism, and purine metabolism. These findings underscore the potential of ADBP as a functional ingredient for food and biomedical applications aimed at the prevention and adjunctive treatment of HUA.

1. Introduction

The prevalence of hyperuricemia (HUA) in China has been steadily increasing, currently affecting approximately 14% of the population. Reducing serum uric acid levels remains the primary strategy for both the prevention and management of this condition[1]. Xanthine oxidase (XOD), a pivotal enzyme in uric acid biosynthesis, plays a central role in the development of HUA and associated oxidative stress, particularly when overexpressed. Although synthetic XOD inhibitors are effective in reducing uric acid production and alleviating HUA, their long-term use is often limited by adverse effects and reduced efficacy over time[2]. In this context, natural bioactive compounds, including peptides, polyphenols, flavonoids, and alkaloids derived from food sources, have emerged as promising alternatives, offering a potentially safer approach to uric acid reduction[3-4]. Among these, peptides derived from enzymatic hydrolysates of fish, shrimp, eggs, meat, rice, and milk proteins offer distinct

[1] Wei Li and Hongliang Chen contributed equally to the work.

* Corresponding author at: Institute of Biopharmaceutical and Health Engineering, Tsinghua Shenzhen International Graduate School, Shenzhen 518055, China
E-mail address: xhxing@tsinghua.edu.cn

Peer review under responsibility of Beijing Academy of Food Sciences.

SciOpen Publishing services by Tsinghua University Press

http://doi.org/10.26599/FSHW.2025.9250796

advantages, including favorable safety profiles, high bioavailability, and significant therapeutic efficacy. These peptides exert antihyperuricemic effects through various mechanisms, such as XOD inhibition, modulation of urate transporters, and regulation of gut microbiota composition[5-7]. Consequently, they represent promising candidates for adjunctive therapy in the clinical management of HUA.

Andrias davidianus, commonly known as the Chinese giant salamander, is the largest extant amphibian and has long been valued for its nutritional and medicinal properties[8]. In response to conservation efforts, artificial farming practices have been widely adopted, transforming the species into a significant aquaculture resource, leading to surplus production. Various parts of *A. davidianus*, including meat, bones, skin, liver, blood, and tail fat, have been recognized for their potential health benefits, both dietary and therapeutic[9]. Our previous studies have focused on bioactive peptides extracted from the meat, bones, and skin of *A. davidianus*. Among these, peptides derived from *A. davidianus* bones (ADBP) have been identified as a complex mixture exhibiting potent XOD inhibitory activity *in vitro*, along with nephroprotective effects *in vivo*[10-12]. Despite these promising results, the antihyperuricemic potential of ADBP derived from different farming regions has yet to be systematically evaluated. Given the heterogeneous nature of ADBP, its composition is likely influenced by various factors, including geographical location, environmental conditions, animal age, and genetic background. These variables can significantly alter both the peptide profile and bioactivity, highlighting the need for the establishment of rigorous quality control standards. To date, however, no standardized quality control framework for ADBP from different origins has been reported, impeding both research progress and commercial application. To facilitate more comprehensive investigations and support the transition of ADBP to clinical and industrial use, the development of a robust quality control protocol is essential. Establishing such standards could also contribute to the economic sustainability of endemic Chinese species, while promoting conservation efforts and advancing the artificial breeding industry for the Chinese giant salamander. High-performance liquid chromatography (HPLC) fingerprinting has proven to be an effective analytical technique for profiling complex biological mixtures, allowing for the detection of both known and unknown constituents[13]. This method has been widely applied in the quality evaluation of protein hydrolysates and plant-based extracts, such as corn peptides, chicken collagen peptides, and *Phyllanthus emblica*[14-17].

To support the development and application of ADBP as a functional food ingredient with antihyperuricemic potential, the present study was designed with three primary objectives: 1) to conduct a comprehensive quality assessment of ADBP obtained from 9 distinct farming regions; 2) to develop a reliable HPLC fingerprinting method for ADBP characterization; and 3) to evaluate the *in vitro* and *in vivo* antihyperuricemic activities of the most bioactive ADBP samples.

2. Materials and methods

2.1 Reagents

Alkaline protease (200 000 U/g) was purchased from Beijing Donghua Qiangsheng Biotechnology Co., Ltd. (Beijing, China). LO_2 cells were obtained from Procell Life Science & Technology Co., Ltd. (Wuhan, China). Bicinchoninic acid (BCA), uric acid, alanine aminotransferase (ALT), aspartate aminotransferase (AST), adenosine deaminase (ADA), XOD, superoxide dismutase (SOD), catalase (CAT), glutathione (GSH), and malondialdehyde (MDA) were supplied by Jiancheng Biotechnology Institute (Nanjing, China). XOD, uric acid, hypoxanthine, xanthine, inosine, adenosine, potassium oxonate, and allopurinol were obtained from Sigma-Aldrich (Steinheim, Germany). All other reagents were of analytical grade.

2.2 Preparation and HPLC fingerprinting of ADBP

2.2.1 ADBP sample preparation

Bones from artificially cultivated *A. davidianus* (5 years old, 2.5–3.5 kg) were collected from 9 provinces in China, with details provided in Table S1. Habitat codes were assigned as follows: HBES (Enshi, Hubei); SXHZ (Hanzhong, Shanxi); HNLY (Luoyang, Henan); JXSR (Shangrao, Jiangxi); GXWZ (Wuzhou, Guangxi); SCYB (Yibin, Sichuan); GZQN (Qiannan, Guizhou); HNZJJ (Zhangjiajie, Hunan); CQYC (Yongchuan, Chongqing). Specimens were identified and supplied by President Songjun Wang of the Henan Giant Salamander Protection and Development Association.

ADBP was prepared using a previously reported method with minor modifications[10]. Bone powder was enzymatically hydrolyzed with alkaline protease at 50 °C and pH 9 for 4 h. The hydrolysate was centrifuged at 5 000 × *g* for 10 min, and the supernatant was freeze-dried to yield ADBP. Quality evaluation of ADBP was conducted, including assessments of extraction yield, XOD inhibitory activity, molecular weight distribution, proximate composition, mineral content, and amino acid profile.

2.2.2 HPLC fingerprinting analysis

Chromatographic conditions: HPLC fingerprinting was performed using an Agilent 1260 Infinity I HPLC-DAD system (Agilent Technologies, Germany). ADBP solutions were injected onto a DIKMA C_{18} column (250 mm × 4.6 mm, 5 μm) maintained at 30 °C, with a flow rate of 1 mL/min. A binary gradient elution was applied, with mobile phase A consisting of 0.5% trifluoroacetic acid (TFA) in water and mobile phase B consisting of 0.5% TFA in acetonitrile. The gradient was programmed as follows: 0–20 min, 0%–5% B; 20–70 min, 5%–25% B. Detection was performed at 220 nm using a diode-array detector (DAD), and the injection volume was set to 20 μL.

Methodology validation: ADBP solutions from Hunan Zhangjiajie (HNZJJ) region were prepared and analyzed to assess the precision, repeatability, and stability of the HPLC fingerprinting method. Precision was determined from 6 successive injections of the same sample. Repeatability was evaluated using 6 separately prepared solutions. Stability was assessed by analyzing a single sample at 0, 2, 4, 6, 8, 12, and 24 h.

Similarity and cluster analysis: The HPLC fingerprints of 9 ADBP solutions were matched using the Similarity Evaluation System for Chromatographic Fingerprints of Traditional Chinese Medicine (Version 2012, Beijing, China). A reference fingerprint was established using the median method, and similarity values were calculated. Inter-sample similarity and variation were assessed through hierarchical clustering analysis (HCA) using OmicStudio tools (https://www.omicstudio.cn/tool).

2.3 In vitro uric acid-lowering activity and hyperuricemic cell model development

HPLC conditions for purine detection: Purines were analyzed using an Agilent 1260 Infinity I HPLC-DAD system (Agilent Technologies, Germany) equipped with a DIKMA C_{18} column (250 mm × 4.6 mm, 5 μm). A binary gradient elution was applied, with mobile phase A consisting of 0.05 mmol/L KH_2PO_4 (pH 4) and mobile phase B composed of methanol. Elution was maintained at 5% B for the first 15 min. The HPLC conditions were as follows: detection at 254 nm, flow rate 1 mL/min, column temperature maintained at 30 ℃, and an injection volume 20 μL. Standard solutions of uric acid, xanthine, hypoxanthine, inosine, and adenosine at varying concentrations were analyzed, and calibration curves were generated accordingly.

Optimization of induction conditions: LO_2 cells were cultured in DMEM/F12 medium supplemented with 10% fetal bovine serum (FBS) and 1% antibiotics (100 U/mL penicillin, 100 μg/mL streptomycin) at 37 ℃ in a humidified incubator with 5% CO_2. A high-uric-acid cell model was developed in LO_2 cells by modifying the method described by Liu et al.[18]. LO_2 cells (2×10^4–10×10^4 cells/well) were seeded in 24-well plates and incubated for 24 h. After removal of the supernatant, adenosine (100–1 000 μg/mL) was added to the experimental group for 12–48 h, while the control group was maintained in basic medium. Induction conditions were optimized by quantifying xanthine and inosine concentrations in the supernatant. To induce uric acid production, XOD was added to convert hypoxanthine and xanthine. The optimal XOD concentration (0.005–0.400 U/mL) and incubation time (0.5–3.0 h) were identified to establish the high-uric-acid model.

For ADBP intervention, LO_2 cells (8×10^4 cells/well) were seeded in 24-well plates and incubated for 24 h. The control and model groups were cultured in basic medium for an additional 24 h, while the experimental group was treated with varying concentrations of ADBP. Adenosine (600 μg/mL) was then added to both the model and experimental groups, while the control group was maintained in fresh basic medium for another 30 h. XOD (0.05 U/mL) was subsequently added to the model and experimental groups. After 1.5 h of incubation, uric acid levels in the supernatant were measured by HPLC.

2.4 In vivo evaluation of antihyperuricemic activity

Animal experiments were performed in accordance with previously established protocols[10]. All procedures were approved by the Ethics Committee of Experimental Animals at Peking University Shenzhen Graduate School (SYXK-2020-0172). Mice were randomly assigned to 6 groups: control, model, allopurinol, and ADBP treatment groups (200, 400, and 800 mg/kg). From days 1 to 7, the control group was administered distilled water and a standard diet, while the other groups were gavaged with potassium oxonate (100 mg/kg day) and fed a 0.2% adenine-containing diet. Starting on day 1, 1 h after PO administration, the control and model groups received distilled water daily for 3 weeks, while the allopurinol group was treated with allopurinol (20 mg/kg·day), and the ADBP groups received ADBP at doses of 200, 400, or 800 mg/kg. On day 28, body weights were recorded, and all mice were euthanized. Livers were collected, photographed, and weighed for liver index calculation. Portions of liver tissue were fixed in 4% paraformaldehyde for histopathological and immunohistochemical analysis, while the remaining samples were stored at –80 ℃ for subsequent biochemical evaluation.

2.4.1 Biochemical indicators

The levels of uric acidand antioxidant indices (SOD, CAT, GSH, and MDA) in the liver, as well as ALT and AST levels in serum, ADA activity, and XOD activity in both serum and liver, were analyzed using commercial kits obtained from Jiancheng Biotechnology Institute (Nanjing, China).

2.4.2 Histological examination

Liver tissues were collected and fixed in 4% formalin buffer. Following fixation, the tissues were subjected to routine processing, including washing, dehydration, embedding, and sectioning (4 μm). The prepared tissue sections were stained with hematoxylin-eosin (HE) and photographed under a light microscope at 200× magnification.

2.4.3 Immunohistochemistry analysis

Paraffin-embedded liver slices were processed for immunohistochemical analysis as described in our previous report[10]. In brief, liver slices were incubated with primary XDH antibody, followed by incubation with secondary antibodies conjugated to avidin-labelled HRP. The slices were then stained with DAB chromogenic solution. Immunohistochemical images were captured using a light microscope (Leica, Germany), and the resulting images were analyzed using ImageJ software.

2.4.4 Quantitative real-time PCR analysis

Liver tissue samples were collected at the time of sacrifice and stored at –80 ℃ until further use. Total RNA was extracted from the samples, followed by reverse transcription into cDNA and amplification using a CFX96™ real-time system (Bio-Rad, USA) according to the manufacturers' instructions. Relative quantification of target genes was performed using the $2^{-\Delta\Delta ct}$ method, with *GAPDH* used as the internal reference gene. The primers used in the analysis are listed in Table S2 and were obtained from Sangon Biotech (Shanghai, China).

2.4.5 Liver metabolomics analysis

Liver samples were analyzed by Wuhan MetWare Biotechnology (Wuhan, China) for metabolomics analysis, following the approach outlined in our previous study[10]. Briefly, the processed samples were analyzed using an ultra-performance liquid chromatography tandem mass spectrometry (UPLC-MS/MS) system, which couples UPLC (ExionLC AD, https://sciex.com.cn/) with MS/MS (QTRAP®, https://sciex.com.cn/). Separation of metabolites was performed using a Waters ACQUITY UPLC HSS T3 C_{18} column (1.8 μm, 2.1 mm × 100 mm). All metabolomics analyses were conducted according to the standard operating procedures of Wuhan MetWare Biotechnology (Wuhan, China).

2.5 Statistical analysis

All graphs were generated using GraphPad Prism (version 8.0), and data are presented as mean ± standard deviation (SD). Statistical analysis was performed using One-way ANOVA with Dunnett's post hoc test in SPSS PASW Statistics 18.0. Image analysis was conducted using ImageJ. Statistical significance was considered at $P < 0.05$.

3. Results

3.1 Comparative analysis of ADBP from different habitats

3.1.1 Peptide composition

Bone peptides were extracted from *A. davidianus* sourced from 9 farming sites and analyzed for yield and bioactivity. As illustrated in Figs. 1A and B, the extraction yields varied between 37.05% and 49.39%, with the highest yield observed in the CQYC sample ((49.39 ± 1.42)%) and the lowest in the SXHZ sample ((37.05 ± 1.48)%). The sample from HNZJJ region exhibited the second-highest yield, significantly surpassing both those from SXHZ and GXWZ regions ($P < 0.05$). No significant differences were found among the HBES, HNLY, JXSR, SCYB, and GZQN samples ($P > 0.05$). As shown in Fig. 1C, the samples from GZQN and HNZJJ regions demonstrated significantly stronger XOD inhibitory activity compared to the other samples ($P < 0.05$), suggesting their promising antihyperuricemic potential. Overall, these 2 samples exhibited superior extraction efficiency and bioactivity.

To comprehensively compare ADBP from various sources, we analyzed their molecular weight distribution, basic composition, mineral element content, and amino acid profiles. As shown in Fig. 1D, all 9 samples were predominantly composed of low molecular weight peptides (< 3 kDa), accounting for approximately 99% of the total peptides. Among them, HBES sample contained the highest proportion of peptides < 1 kDa ((86.32 ± 0.83)%), while HNLY sample had the lowest proportion ((81.00 ± 1.72)%). No significant differences were observed among the other samples ($P > 0.05$). In contrast, HNLY sample exhibited a significantly higher proportion of peptides in the 1–3 kDa range ((18.53 ± 1.22)%) compared to HBES ((13.62 ± 0.91)%), JXSR ((14.88 ± 0.89)%), GZQN ((14.19 ± 1.38)%), and HNZJJ ((14.65 ± 1.22)%) samples ($P < 0.05$), though no significant differences were found between HNLY sample and the remaining samples ($P > 0.05$). Overall, peptides < 3 kDa constituted the dominant fraction in all samples. Basic compositional analysis (Figs. 1E-H) revealed moisture contents ranging from (6.51 ± 1.01)% to (8.88 ± 0.45)%. Protein content was consistently around 80% across all samples, ranging from (76.59 ± 1.32)% to (81.61 ± 0.96)%. Fat content was significantly higher in GZQN, HNZJJ, and CQYC samples ($P < 0.05$), while HNLY sample had the lowest fat content ((0.48 ± 0.03%)) ($P < 0.05$). Ash content was highest in SXHZ sample and lowest in HNLY and HNZJJ samples.

Elemental analysis (Fig. 1I-N) indicated significantly higher K and Ca levels in CQYC and HNLY samples, with the lowest levels found in GZQN and HNZJJ samples ($P < 0.05$). P content ranged from 563 to 1 088.67 mg/kg, with CQYC sample having nearly double the phosphorus content compared to GZQN and HNZJJ samples ($P < 0.05$). Fe levels in SXHZ, GXWZ, and SCYB samples were approximately twice as high as those in JXSR, GZQN, HNZJJ, and CQYC samples ($P < 0.05$). Zn was most abundant in SCYB sample, followed by HNLY sample, and lowest in CQYC sample ($P < 0.05$), with no significant differences among the other samples ($P > 0.05$). Se levels ranged from 0.31 to 0.97 mg/kg, all exceeding the threshold for selenium-enriched agricultural products in China (> 0.15 mg/kg, ICS CCS GH/T 1135–2024). GXWZ, JXSR, and HBES samples had Se levels nearly 3 times higher than SCYB and CQYC samples ($P < 0.05$), with no significant differences among the other groups. Amino acid profiles (Table 1) varied across the different regions. HBES sample had the highest glycine content; SXHZ sample had the highest levels of valine, isoleucine, tyrosine, and histidine; GXWZ sample was richest in threonine; HNZJJ sample had the highest concentrations of alanine, leucine, phenylalanine, methionine, serine, aspartic acid, glutamic acid, lysine, and arginine; and CQYC sample exhibited the highest proline content. These regional differences influenced the levels of hydrophobic amino acids (HAA), essential amino acids (EAA), and total amino acids (TAA). HAA content was significantly higher in HNZJJ ((23.05 ± 0.45) g/100 g) and CQYC ((22.14 ± 0.38) g/100 g) samples ($P < 0.05$), with no notable differences among other samples ($P > 0.05$). EAA content was significantly higher in HNZJJ ((19.52 ± 0.39) g/100 g) and SXHZ ((18.21 ± 0.59) g/100 g) samples ($P < 0.05$), while TAA was the highest in HNZJJ sample ((68.69 ± 1.78) g/100 g), followed by CQYC sample ((65.96 ± 1.37) g/100 g) ($P < 0.05$). In conclusion, HNZJJ and CQYC samples exhibited the most favorable amino acid profiles, with significantly higher levels of HAA, EAA, and TAA compared to the other sources.

In total, ADBP derived from HNZJJ and CQYC regions were identified as the optimal samples for the potential prevention of HUA, based on their extraction efficiency, XOD inhibitory activity, and compositional analysis. Notably, HNZJJ is a key production area for the artificial breeding of *A. davidianus* in China. Given the promising application of ADBP in the adjunctive therapy for HUA management, ADBP from HNZJJ region was selected for further efficacy evaluation.

3.1.2 HPLC fingerprint profiles

The HNZJJ sample was employed to validate the analytical method. To assess intraday precision, repeatability, and stability, the relative standard deviations (RSD) of relative retention times (RRT) and relative peak areas (RPA) for 13 characteristic peaks (using peak 7 as the reference) were evaluated. Intraday precision yielded RRT and RPA variations ranging from 0.06% to 0.80% and 0.96% to 3.64%, respectively, confirming the excellent performance of the instrument. Repeatability tests showed RRT and RPA variations of less than 1% and 3%, respectively, demonstrating strong reproducibility. Stability over 48 h was confirmed by RRT and RPA variations within the ranges of 0.03% to 0.55% and 0.64% to 3.42%, respectively.

HPLC fingerprints of ADBP samples from nine habitats were analyzed using the Traditional Chinese Medicine Chromatographic Fingerprint Similarity Evaluation System (version 2012). As shown in Fig. 2, 13 of the 22 common peaks (selected for their resolution and abundance) were identified as characteristic. Peak 7, chosen for its moderate retention time and high abundance, served as the reference for calculating RRT and RPA. The RRT RSDs were consistently low, ranging from 0.05% to 0.67%, while RPA exhibited broader variation (10.10% to 32.53%, Table S3), reflecting differences in peak concentrations across samples. Similarity analysis revealed high correlation coefficients (0.969–0.997) among the samples (Table S4),

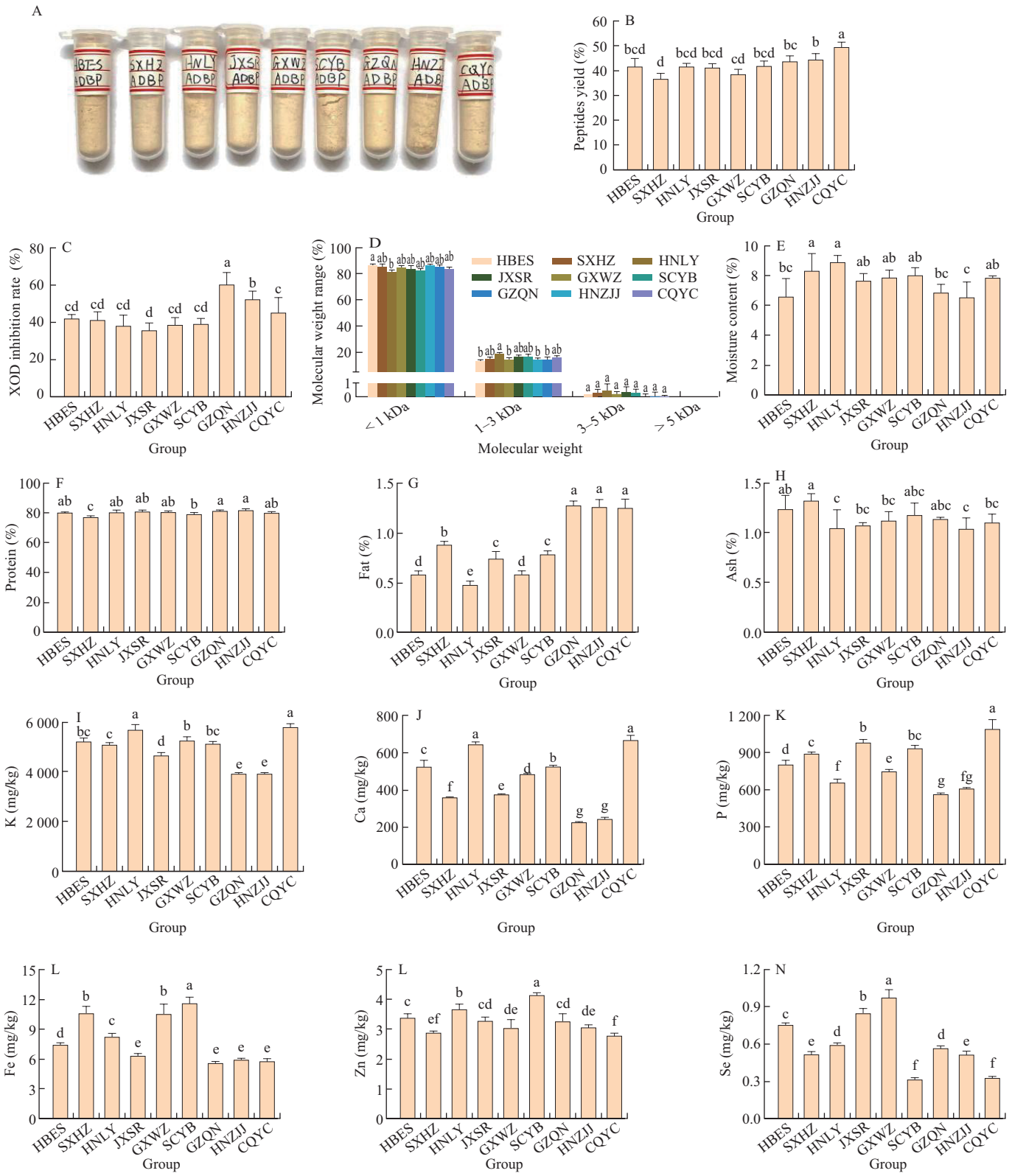

Fig. 1 Extraction and compositional analysis of ADBP from nine habitats ($n = 3$). (A) ADBP samples from different geographic sources; (B) Peptide yield; (C) XOD inhibition rate; (D) Molecular weight distribution; (E) Moisture content; (F) Protein content; (G) Fat content; (H) Ash content; (I-N) K, Ca, P, Fe, Zn and Se content. Different lowercase letters indicate significant difference ($P < 0.05$).

Table 1
Amino acid compositions and contents of ADBP from 9 habitats ($n = 3$).

Amino acids	Enshi, Hubei	Hanzhong, Shanxi	Luoyang, Henan	Shangrao, Jiangxi	Wuzhou, Guangxi	Yibin, Sichuan	Qiannan, Guizhou	Zhangjiajie, Hunan	Yongchuan, Chongqing
Gly	11.58 ± 0.92^{a}	8.16 ± 0.12^{d}	11.20 ± 0.46^{a}	10.98 ± 0.43^{ab}	9.48 ± 0.21^{c}	9.95 ± 0.4^{c}	10.23 ± 0.21^{bc}	10.85 ± 0.53^{ab}	11.10 ± 0.34^{a}
Ala	4.16 ± 0.18^{bc}	3.81 ± 0.05^{d}	4.14 ± 0.17^{bc}	4.11 ± 0.06^{bc}	4.03 ± 0.09^{cd}	3.96 ± 0.13^{cd}	4.07 ± 0.08^{bc}	4.41 ± 0.18^{a}	4.3 ± 0.10^{ab}
Val	2.29 ± 0.14^{c}	2.71 ± 0.15^{a}	2.31 ± 0.12^{c}	2.46 ± 0.18^{bc}	2.51 ± 0.15^{abc}	2.43 ± 0.13^{bc}	2.46 ± 0.06^{bc}	2.60 ± 0.14^{ab}	2.51 ± 0.07^{abc}
Leu	4.26 ± 0.18^{bc}	4.44 ± 0.1^{ab}	4.27 ± 0.1^{bc}	4.13 ± 0.09^{cd}	4.31 ± 0.14^{bc}	3.98 ± 0.16^{d}	4.10 ± 0.11^{cd}	4.59 ± 0.11^{a}	4.24 ± 0.12^{bc}
Ile	1.87 ± 0.09^{bc}	2.18 ± 0.1^{a}	1.80 ± 0.04^{c}	1.94 ± 0.06^{bc}	1.99 ± 0.11^{b}	1.94 ± 0.06^{bc}	1.93 ± 0.06^{bc}	1.98 ± 0.09^{b}	1.94 ± 0.09^{bc}
Pro	5.46 ± 0.19^{b}	4.43 ± 0.17^{d}	5.72 ± 0.18^{a}	5.44 ± 0.18^{b}	4.81 ± 0.05^{c}	5.27 ± 0.16^{b}	5.42 ± 0.10^{b}	5.76 ± 0.13^{a}	5.79 ± 0.05^{a}
Phe	2.06 ± 0.04^{a}	2.24 ± 0.05^{a}	1.98 ± 0.18^{bc}	2.03 ± 0.07^{bc}	1.69 ± 0.52^{c}	2.00 ± 0.09^{bc}	2.06 ± 0.04^{a}	2.28 ± 0.11^{a}	2.15 ± 0.08^{a}
Met	1.24 ± 0.08^{bc}	1.3 ± 0.07^{c}	1.13 ± 0.1b^{c}	1.14 ± 0.08^{bc}	1.33 ± 0.07^{bc}	1.24 ± 0.06^{c}	1.16 ± 0.05^{bc}	1.43 ± 0.11^{a}	1.21 ± 0.07^{b}
Tyr	1.13 ± 0.06^{cd}	1.61 ± 0.06^{a}	1.09 ± 0.03^{d}	1.25 ± 0.06^{bc}	1.59 ± 0.12^{a}	1.27 ± 0.11^{b}	1.37 ± 0.04^{b}	1.56 ± 0.06^{a}	1.29 ± 0.06^{b}
Ser	3.44 ± 0.23^{bc}	3.32 ± 0.09^{c}	3.53 ± 0.11^{bc}	3.46 ± 0.17^{bc}	3.53 ± 0.16^{bc}	3.31 ± 0.14^{c}	3.53 ± 0.06^{bc}	3.93 ± 0.09^{a}	3.67 ± 0.10^{b}
Thr	2.13 ± 0.09^{bc}	2.36 ± 0.17^{b}	2.12 ± 0.07^{bc}	2.17 ± 0.03^{bc}	2.47 ± 0.16^{a}	2.13 ± 0.09^{c}	2.19 ± 0.04^{bc}	2.36 ± 0.10^{b}	2.23 ± 0.06^{b}
Asp	5.59 ± 0.21^{bcd}	5.76 ± 0.05^{bc}	5.44 ± 0.15^{d}	5.39 ± 0.22^{d}	5.54 ± 0.19^{cd}	5.48 ± 0.18^{cd}	5.49 ± 0.12^{cd}	6.13 ± 0.11^{a}	5.86 ± 0.10^{ab}
Glu	8.96 ± 0.25^{c}	9.25 ± 0.15^{bc}	9.27 ± 0.17^{bc}	9.23 ± 0.22^{bc}	9.19 ± 0.19^{bc}	9.26 ± 0.34^{bc}	9.22 ± 0.17^{bc}	10.06 ± 0.34^{a}	9.54 ± 0.20^{b}
Lys	3.74 ± 0.1^{bc}	4.26 ± 0.1^{a}	3.61 ± 0.06^{c}	3.94 ± 0.17^{b}	4.23 ± 0.17^{a}	3.81 ± 0.2b^{c}	3.74 ± 0.06^{bc}	4.27 ± 0.15^{a}	3.93 ± 0.10^{b}
Arg	4.57 ± 0.44^{bc}	4.41 ± 0.22^{c}	4.88 ± 0.1^{abc}	4.83 ± 0.24^{abc}	4.58 ± 0.28^{bc}	4.58 ± 0.31^{bc}	4.67 ± 0.10^{bc}	5.22 ± 0.16^{a}	4.99 ± 0.18^{ab}
His	1.12 ± 0.06^{c}	1.34 ± 0.11^{a}	1.13 ± 0.06^{c}	1.30 ± 0.12^{ab}	1.20 ± 0.06^{abc}	1.16 ± 0.08^{bc}	1.23 ± 0.09^{abc}	1.27 ± 0.10^{abc}	1.22 ± 0.06^{abc}
HAA	21.34 ± 0.29^{bc}	21.10 ± 0.68^{bc}	21.36 ± 0.41^{bc}	21.24 ± 0.67^{bc}	20.66 ± 0.77^{c}	20.83 ± 0.70^{c}	21.21 ± 0.35^{bc}	23.05 ± 0.45^{a}	22.14 ± 0.38^{ab}
EAA	17.59 ± 0.30^{bcd}	19.49 ± 0.53^{a}	17.23 ± 0.48^{d}	17.81 ± 0.44^{bcd}	18.52 ± 0.60^{b}	17.54 ± 0.74^{cd}	17.65 ± 0.27^{bcd}	19.52 ± 0.39^{a}	18.21 ± 0.59^{bc}
TAA	63.59 ± 1.20^{bc}	61.59 ± 1.26^{c}	63.63 ± 1.36^{bc}	63.79 ± 1.25^{bc}	62.47 ± 0.63^{c}	61.78 ± 2.44^{c}	62.89 ± 1.09^{c}	68.69 ± 1.78^{a}	65.96 ± 1.37^{b}

Note: Different lowercase letters indicate significant difference ($P < 0.05$).

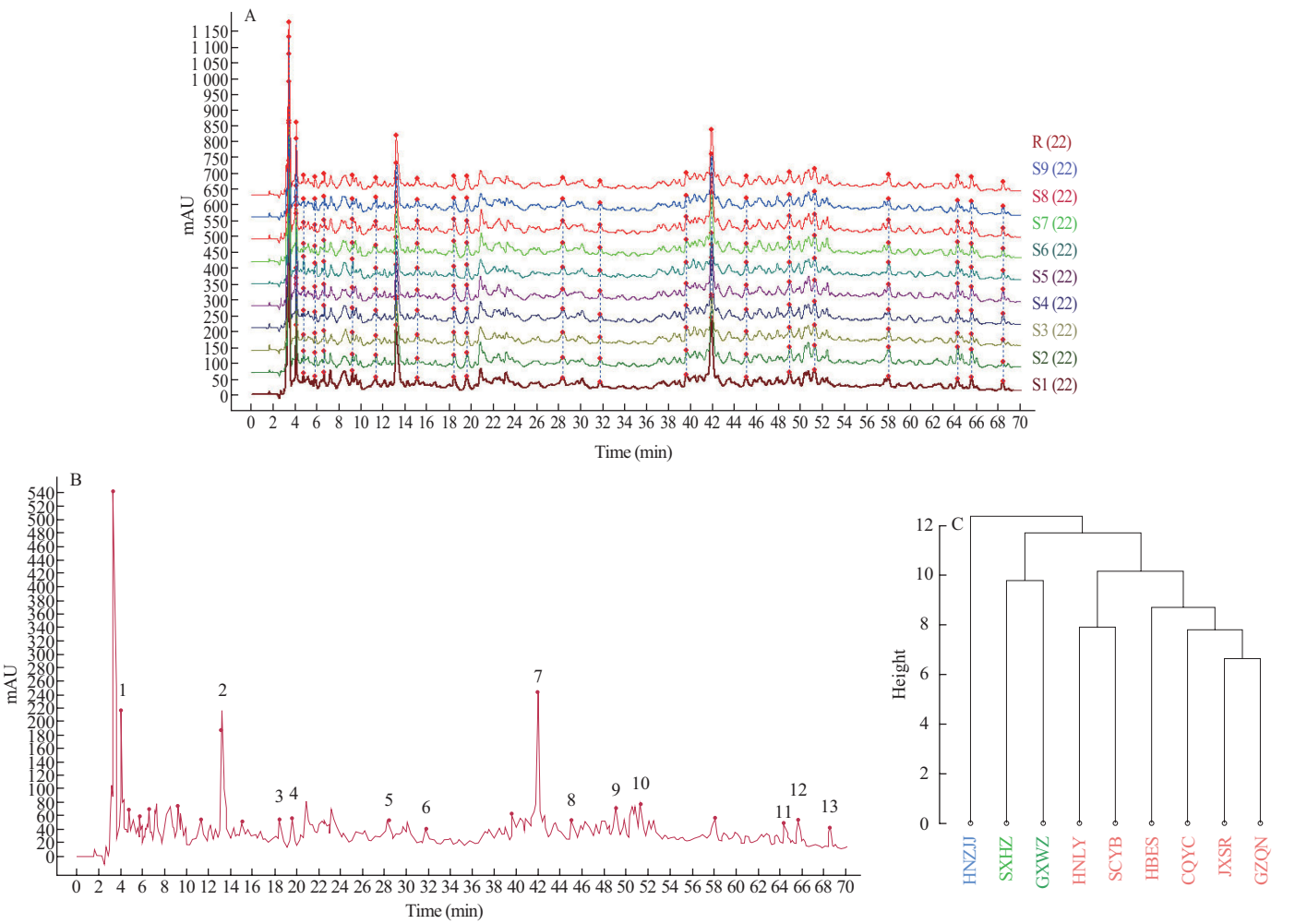

Fig. 2 HPLC fingerprint profiles of ADBP from 9 habitats and hierarchical clustering analysis ($n = 3$). (A) Chromatographic fingerprints of ADBP samples from 9 regions; (B) Reference fingerprint generated from average chromatograms; (C) Cluster analysis based on peptide composition and HPLC data. S1–S9 represent ADBP samples from HBES, SXHZ, HNLY, JXSR, GXWZ, SCYB, GZQN, HNZJJ, and CQYC regions, respectively. R denotes the reference fingerprint. Peaks 1–22 indicate common peaks across all samples.

indicating consistent chemical profiles and validating the fingerprint as a reliable quality standard. HCA grouped the samples into 3 clusters at a similarity threshold of 10: branch 1 contained only HNZJJ sample, distinctly separated; branch 2 grouped SXHZ and GXWZ samples; and branch 3 included the remaining 6 samples. In conclusion, a robust HPLC fingerprint for ADBP from diverse sources was established, with the chemically distinct HNZJJ sample selected for subsequent antihyperuricemic activity studies.

3.2 Uric acid-lowering effect of ADBP obtained from HNZJJ region in a hyperuricemic LO_2 cell model

An LO_2 cell model of HUA was established to assess the uric acid-lowering effects of ADBP. Adenosine, a precursor of uric acid, is metabolized into hypoxanthine and inosine, which are further converted to uric acid. To optimize precursor generation, adenosine concentration, cell density, and incubation time were systematically varied, followed by conversion to uric acid via exogenous XOD. As shown in Figs. $3A_1$ and A_4, increasing the adenosine concentration elevated the levels of hypoxanthine and inosine in the supernatant. Incubation with 600 μg/mL adenosine for 24 h produced high levels of precursors with minimal residual adenosine, making this condition optimal. Increasing the cell density reduced residual adenosine (Fig. $3B_3$) while significantly increasing precursor concentrations (Figs. $3B_1$ and B_3). At a cell density of 8×10^4 cells/mL, precursor levels plateaued, and adenosine depletion reached its maximum, thus defining the optimal cell density. A 30-h incubation further enhanced hypoxanthine accumulation (Figs. $3C_1$-C_4). Using these optimized parameters (600 μg/mL adenosine, 8×10^4 cells/mL, 30 h),

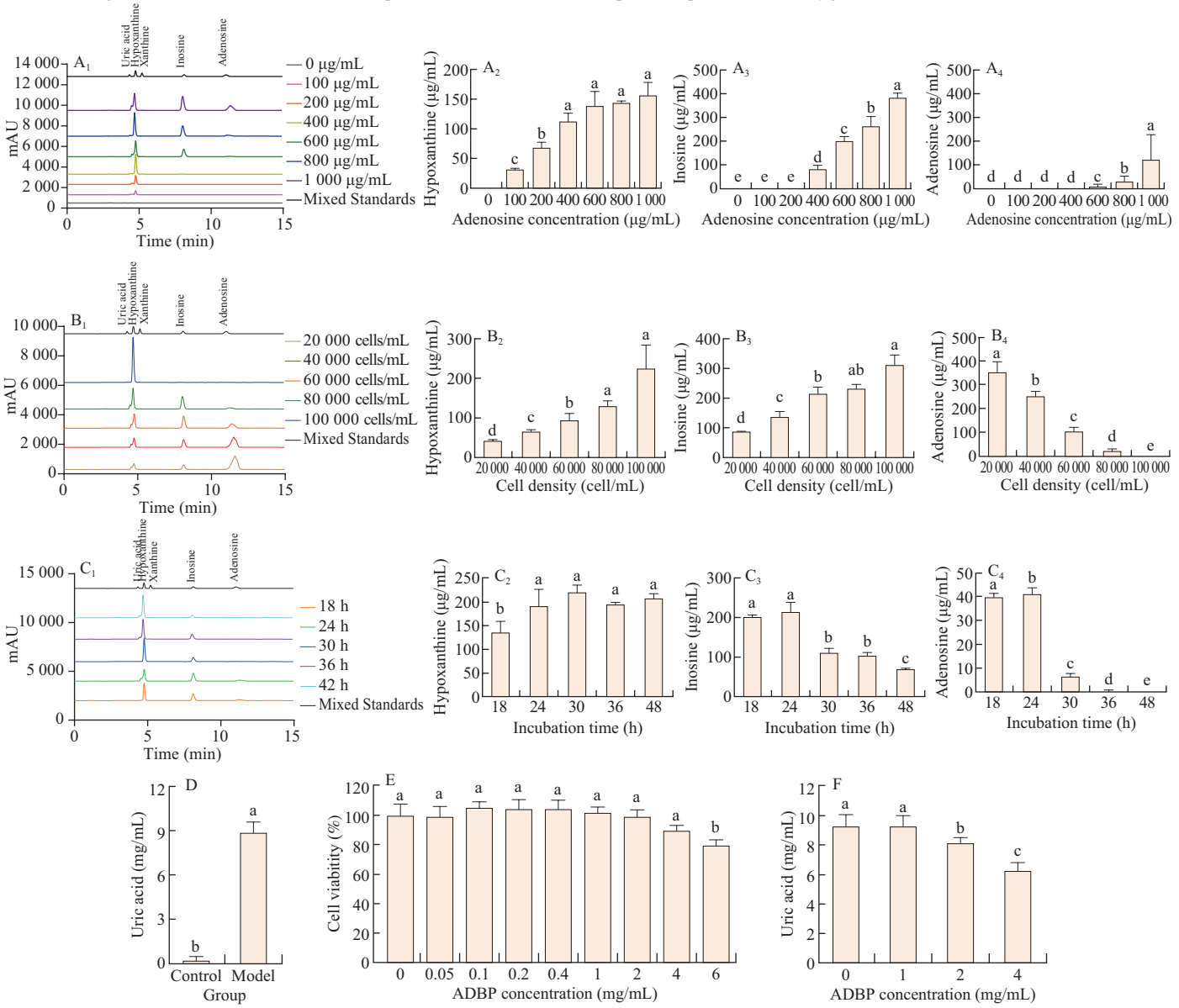

Fig. 3 Optimization of induction conditions for the LO_2 HUA cell model and the uric acid-lowering effect of ADBP obtained from HNZJJ region ($n = 3$). (A_1) Purine base profiles in LO_2 cell supernatants following adenosine induction (100–1 000 μg/mL). (A_2-A_4) Levels of hypoxanthine, inosine, and adenosine in the cell supernatants, respectively. (B_1) Effects of varying cell densities (2–10 × 10^4 cells/mL) on purine metabolism. (B_2-B_4) Levels of hypoxanthine, inosine, and adenosine in the cell supernatants, respectively. (C_1) Influence of incubation time (12–48 h) on purine base production. (C_2-C_4) Levels of hypoxanthine, inosine, and adenosine in the cell supernatants, respectively. (D) Establishment of the HUA model. (E) Cell viability following ADBP treatment. (F) *In vitro* uric acid-lowering effect of ADBP. Statistical analysis was conducted using One-way ANOVA with Dunnett's post hoc test in SPSS PASW Statistics 18.0. Different lowercase letters indicate significant difference ($P < 0.05$).

0.05 U/mL XOD was added for 3 h to convert the precursors into uric acid. As shown in Fig. 3D, uric acid levels significantly increased compared to the control group, confirming the successful establishment of the high-uric-acid LO_2 cell model.

The efficacy of ADBP was then evaluated in this model. ADBP exhibited no cytotoxicity at concentrations up to 4 mg/mL ($P > 0.05$, Fig. 3E), and therefore, 1, 2, and 4 mg/mL doses were selected for further testing. ADBP reduced uric acid levels in a dose-dependent manner compared to the model group ($P < 0.05$, Fig. 3F), demonstrating its effective uric acid-lowering activity in the adenosine-induced HUA LO_2 cell model.

3.3 Antihyperuricemic effects of ADBP obtained from HNZJJ region in HUA mice

3.3.1 Effects on liver function

HUA induces oxidative stress and impairs liver function[19]. As shown in Figs. 4A and B, serum ALT and AST levels were significantly elevated in the model group compared to the control group ($P < 0.05$), indicating liver damage likely caused by a high-purine diet. Treatment with ADBP effectively reduced the levels of these enzymes. Similarly, the liver index was elevated in the model group but was significantly restored with mid- and high-dose ADBP treatment ($P < 0.01$, Fig. 4C). Histological examination revealed hepatomegaly, inflammatory infiltration, and sinusoidal dilation in the model group (Figs. 4D and E). These pathological alterations were markedly alleviated following ADBP treatment, further confirming its hepatoprotective effect in hyperuricemic mice.

3.3.2 Effects on hepatic uric acid biosynthesis

The anti-hyperuricemic effects of ADBP were evaluated by measuring key hepatic enzymes involved in uric acid synthesis in hyperuricemic mice. As shown in Figs. 5A-C, the model group exhibited significantly elevated hepatic uric acid levels and increased activities of XOD and ADA compared to the control group ($P < 0.05$), confirming successful induction of HUA. Allopurinol significantly inhibited XOD activity, resulting in a reduction of hepatic uric acid levels ($P < 0.05$). Similarly, medium and high doses of ADBP significantly reduced hepatic XOD and ADA activities, leading to a decrease in uric acid accumulation ($P < 0.05$). Immunohistochemical analysis revealed pronounced XOD expression in the liver of the model group, which was notably diminished following treatment with medium- and high-dose ADBP (Figs. 5D and E, $P < 0.05$). Additionally, serum activities of XOD and ADA, which were elevated in the model group, were effectively normalized by ADBP administration (Figs. 5F and G, $P < 0.05$). Collectively, these findings demonstrate that ADBP alleviates hepatic uric acid accumulation in hyperuricemic mice, primarily through the inhibition of XOD and ADA activities.

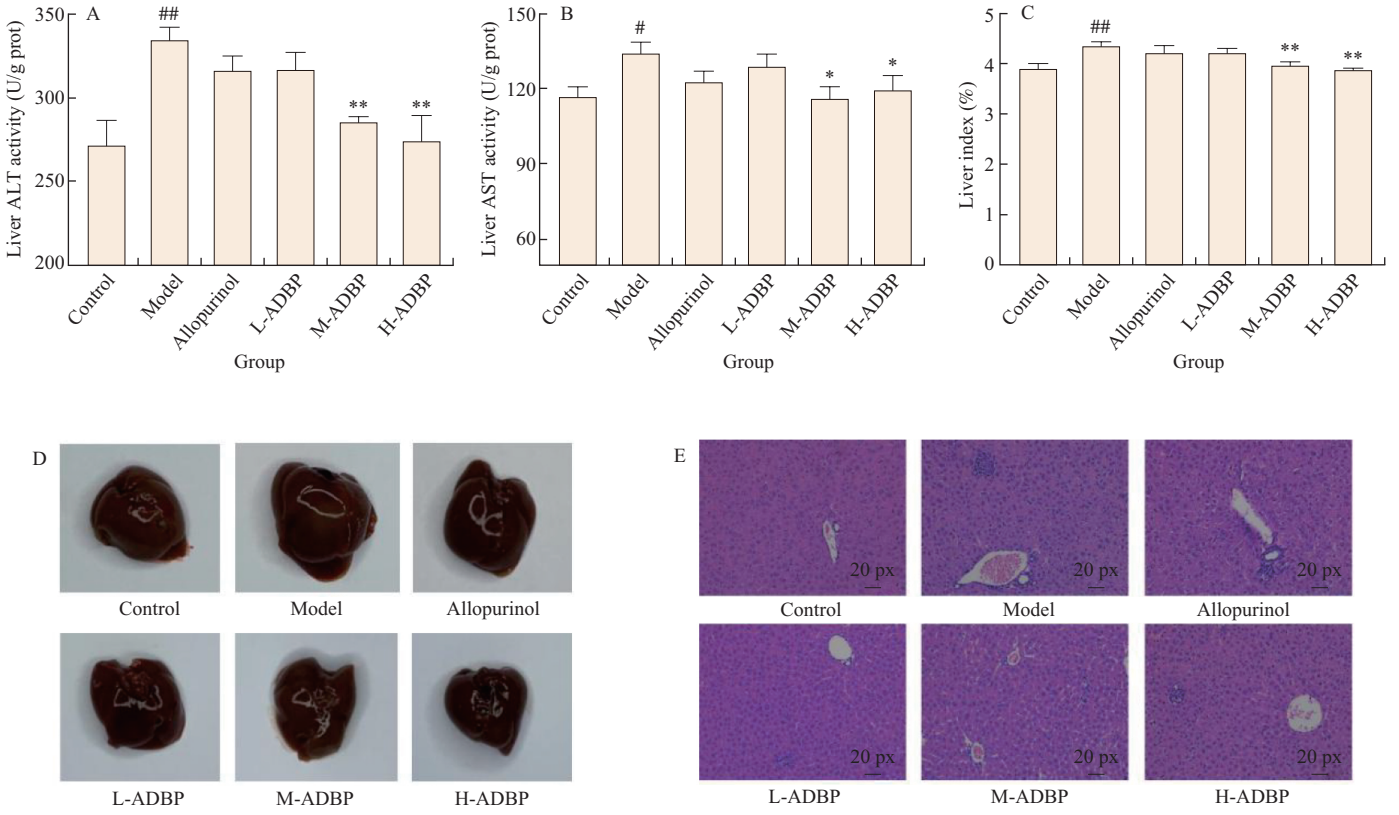

Fig. 4 Effect of ADBP obtained from HNZJJ region on liver function in hyperuricemic mice ($n = 6$). (A) ALT activity. (B) AST activity. (C) Liver index. (D) Liver morphology. (E) Histopathological analysis of liver tissue by PAS staining. L-ADBP, low dose of *A. davidianus* bone peptides; M-ADBP, medium dose of *A. davidianus* bone peptides; H-ADBP, high dose of *A. davidianus* bone peptides, the same below. Statistical analysis was conducted using One-way ANOVA with Dunnett's *post hoc* test in SPSS PASW Statistics 18.0. $^{\#}P < 0.05$, $^{\#\#}P < 0.01$, control group *vs*. Model group; $^{*}P < 0.05$, $^{**}P < 0.01$, Model group *vs*. ADBP group.

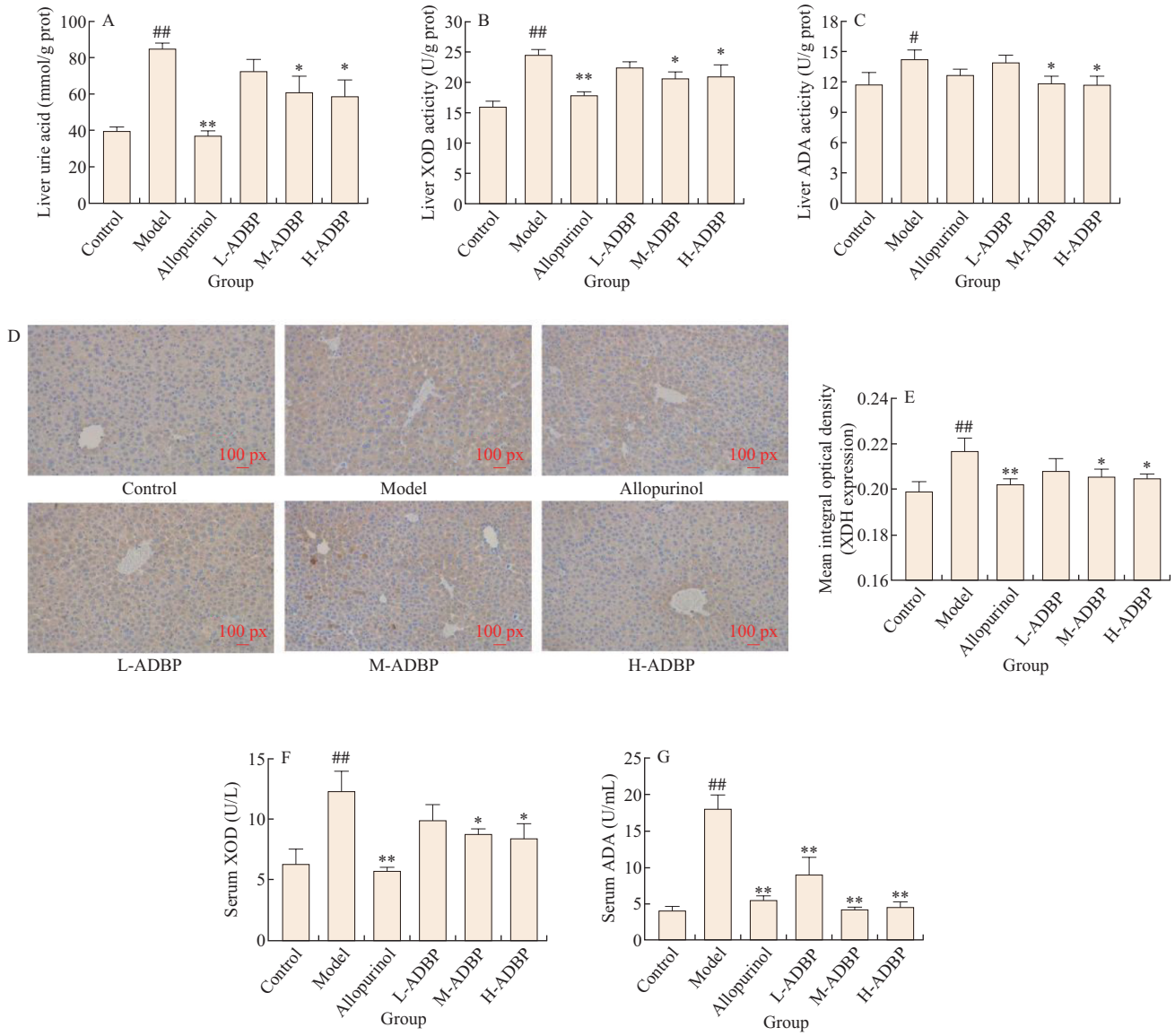

Fig. 5 Effect of ADBP obtained from HNZJJ region on hepatic uric acid biosynthesis in hyperuricemic mice ($n = 6$). (A) Liver uric acid levels; (B) Liver XOD activity; (C) Liver ADA activity; (D) Liver immunohistochemical result of XDH expression; (E) Protein expression of XDH in liver tissue; (F) Serum XOD activity; (G) Serum ADA activity. Statistical analysis was conducted using One-way ANOVA with Dunnett's post hoc test in SPSS PASW Statistics 18.0. $^{\#}P < 0.05$, $^{\#\#}P < 0.01$, control group *vs*. Model group; $^{*}P < 0.05$, $^{**}P < 0.01$, Model group *vs*. ADBP group.

3.3.3 *Effects on hepatic antioxidant activity*

Excess hepatic uric acid in HUA mice induces oxidative stress, leading to liver damage. As shown in Figs. 6A-D, the model group exhibited significantly reduced activities of SOD and CAT, decreased GSH levels, and elevated MDA levels, indicating substantial oxidative injury ($P < 0.05$). These effects were dose-dependently reversed by ADBP treatment ($P < 0.05$). To further validate the hepatoprotective role of ADBP, hepatic mRNA expression of antioxidant genes (*sod2*, *cat*, and *gsh1*) was assessed. As illustrated in Figs. 6E-G, ADBP significantly restored the expression of these genes, which had been suppressed in HUA mice ($P < 0.05$). Taken together, these findings demonstrate that ADBP alleviates HUA-induced hepatic oxidative damage by enhancing antioxidant defenses.

3.3.4 *Effects of ADBP on the liver metabolome in HUA mice*

To further investigate the potential mechanisms by which H-ADBP ameliorates HUA in mice, liver metabolomics analysis was performed. Following data processing, a total of 1 172 metabolites were identified in both positive and negative ion modes. Principal component analysis (PCA) plots revealed clear separation between the control, model, and ADBP groups, indicating significant differences in metabolite profiles across all groups and confirming the alleviating effects of ADBP treatment (Fig. 7A). While some overlap in the metabolic profiles of the two groups was observed, distinct differences in metabolic characteristics were evident. Additionally, to provide a more intuitive representation of overall metabolite variations among the 3 groups, a clustering heatmap was generated (Fig. 7B). In summary, ADBP restored the alterations in liver metabolism observed in HUA mice.

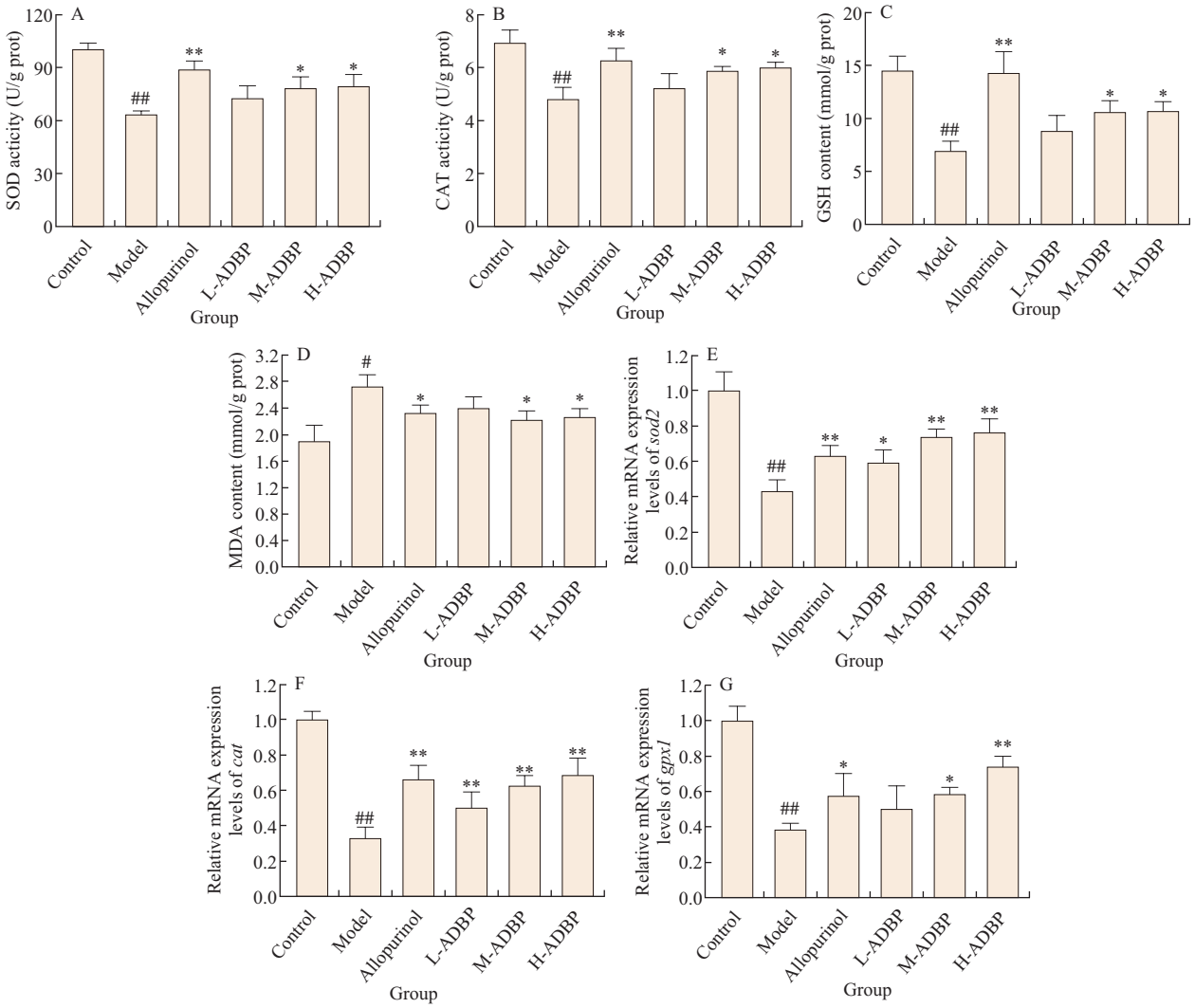

Fig. 6 Effect of ADBP obtained from HNZJJ region on hepatic antioxidant activity and gene expression in hyperuricemic mice ($n = 6$). (A) SOD activity; (B) CAT activity; (C) GSH content; (D) MDA content; (E-G) mRNA expression levels of *sod2*, *cat*, and *gsh1*, respectively. Statistical analysis was conducted using One-way ANOVA with Dunnett's post hoc test in SPSS PASW Statistics 18.0. $^{\#}P < 0.05$, $^{\#\#}P < 0.01$, control group *vs*. Model group; $^{*}P < 0.05$, $^{**}P < 0.01$, Model group *vs*. ADBP group.

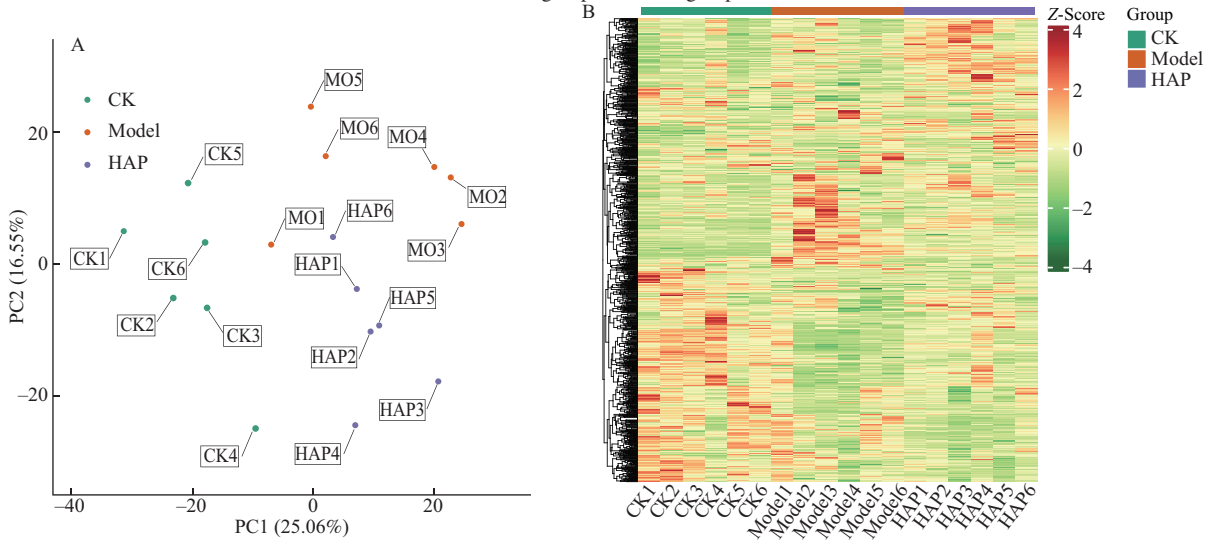

Fig. 7 Effect of ADBP obtained from HNZJJ region on liver metabolism in HUA mice ($n = 6$). (A) PCA of metabolites in liver samples among 3 groups. (B) Hierarchical cluster analysis of overall metabolites variation; (C) Volcano plot of differentially altered metabolites between control and model groups; (D) Volcano plot of differentially altered metabolites between model and ADBP groups; (E) Venn diagram of the distribution of differentially altered metabolites; (F) Hierarchical clustering heatmap of 62 significantly upregulated or downregulated common DEMs. CK, Control group; HAP, H-ADBP group. Bioinformatic analysis was performed using R software and the OmicStudio tools at https://www.omicstudio.cn/tool.

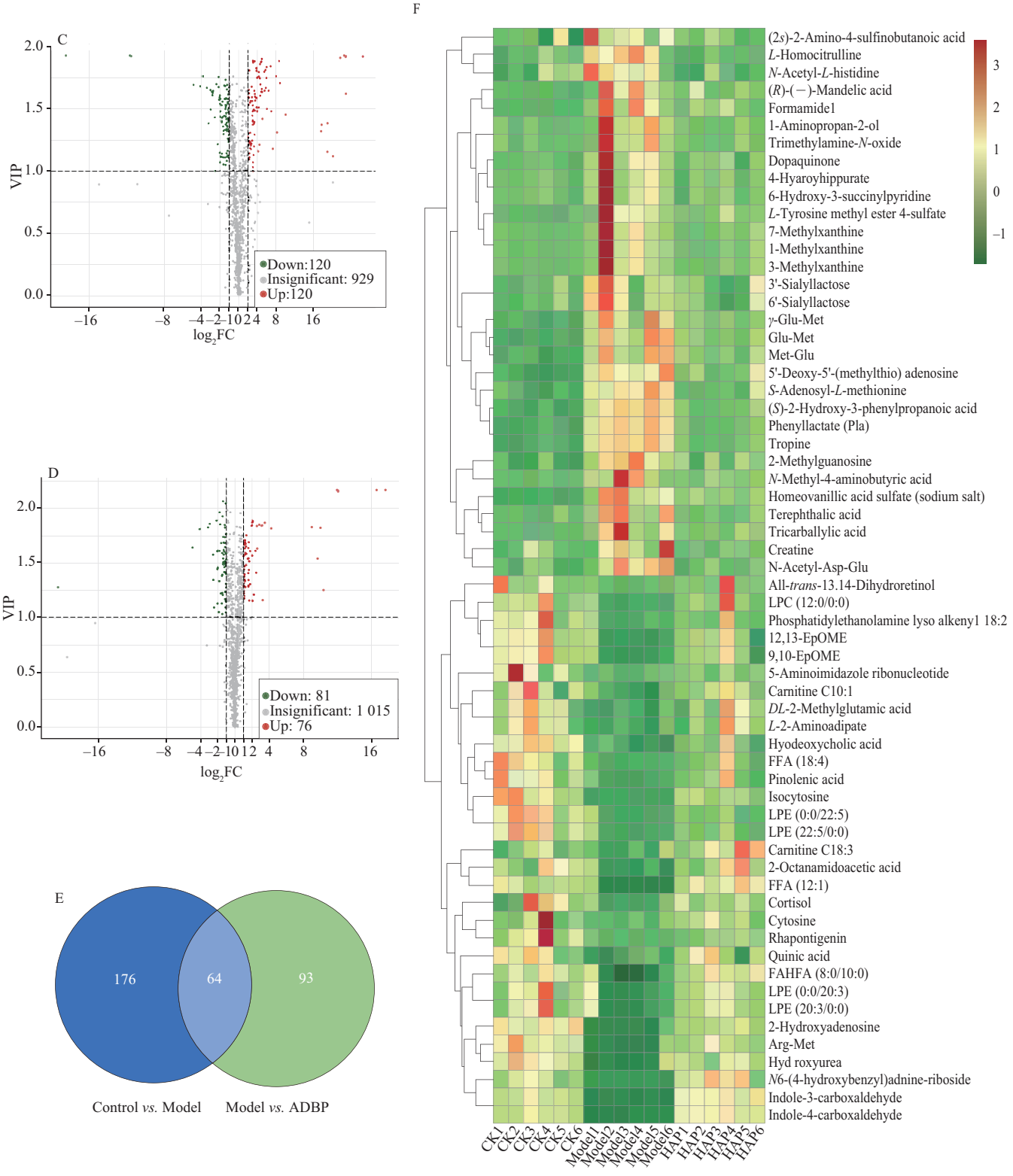

Fig. 7 (*Continued*)

Differential metabolites (DEMs) between the groups were screened using criteria of variable improtance in projection (VIP) ≥ 1 and fold change ≥ 2 or ≤ 0.5. Comparisons between the control and model groups revealed 240 DEMs, consisting of 120 up-regulated and 120 down-regulated metabolites (Fig. 7C). After ADBP intervention, 157 DEMs were identified, including 76 up-regulated and 81 down-regulated metabolites, compared to the model group (Fig. 7D). Notably, 64 metabolites were common to both comparisons (Fig. 7E), of which 62 were restored to levels similar to those in the control group following ADBP treatment, as summarized in Table S5. The cluster heatmaps clearly illustrated the expression levels of these altered metabolites in liver samples, showing distinct differences between the model and ADBP groups, with the latter approaching the control group, thereby demonstrating the efficacy of ADBP treatment (Fig. 7F). These metabolites were classified into 13 different categories at the Class I level, with the predominant classes being amino acids and their metabolites (24.19%), nucleotides and their metabolites (17.74%), organic acids and their derivatives (14.52%), and fatty acids (12.90%) (Fig. 8A). At the Class II level, nucleotides and their metabolites (17.74%), organic acids and their derivatives (14.52%), and amino acid derivatives (12.90%) were the primary components (Fig. 8B). Moreover, the KEGG pathway analysis of these phenotype-related metabolites, conducted using the online MetaboAnalyst 6.0 platform (https://www.metaboanalyst.ca/home.xhtml), revealed that the altered DEMs were enriched in 10 KEGG pathways (Figs. 8C and D). These included linoleic acid metabolism, arginine and proline metabolism, caffeine metabolism, cysteine and methionine metabolism, retinol metabolism, one-carbon pool by folate, alanine, aspartate and glutamate metabolism, lysine degradation, purine metabolism, steroid hormone biosynthesis, and glycine, serine, and threonine metabolism. Notably, 5 pathways, including linoleic acid metabolism, arginine and proline metabolism, caffeine metabolism, cysteine and methionine metabolism, and purine metabolism, were significantly enriched and are closely associated with the therapeutic effects of ADBP in alleviating HUA in mice. Thus, we focus on a detailed discussion of these pathways.

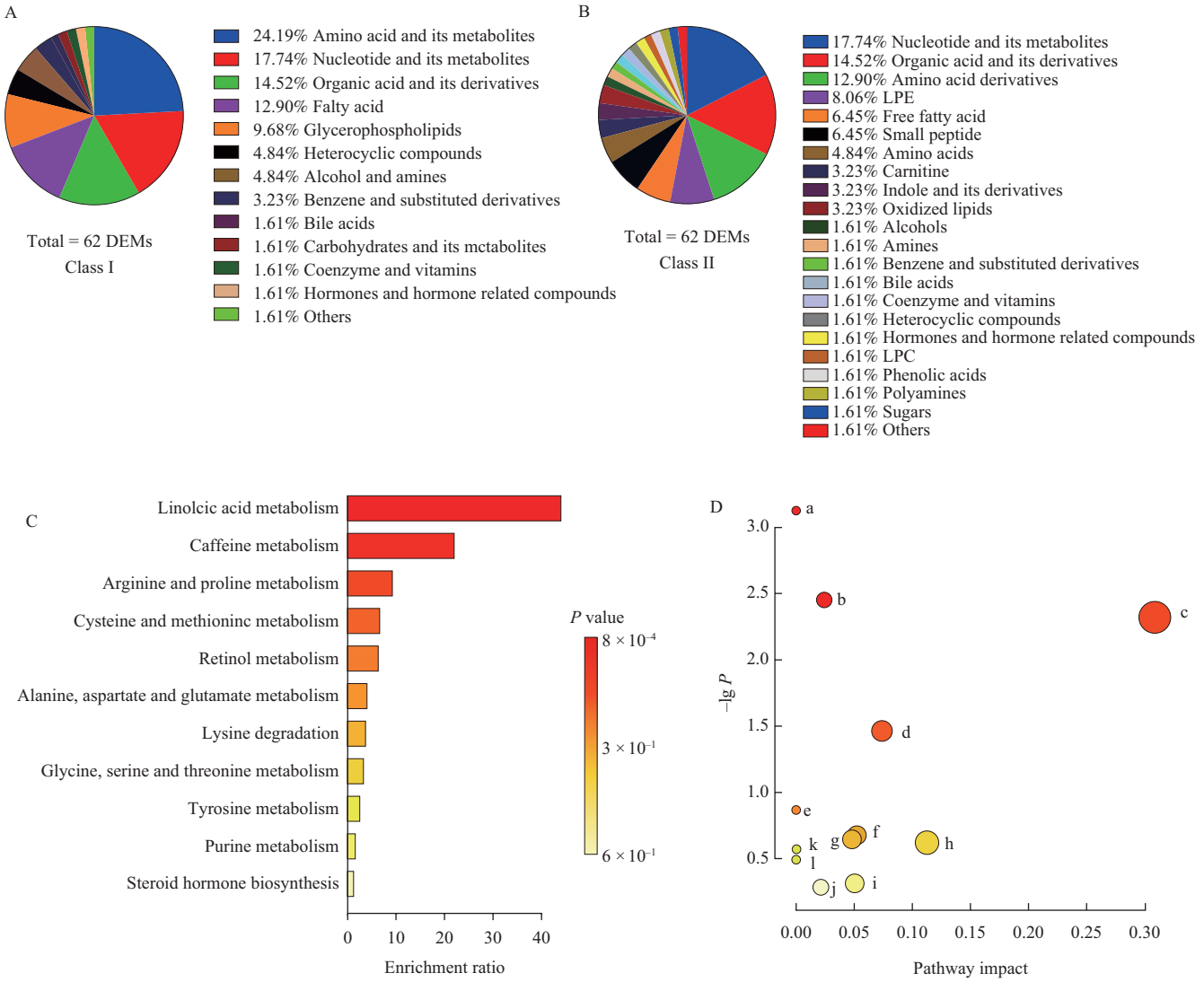

Fig. 8 The pie chart of the classification of significantly altered 62 DEMs at class I (A) and class II (B) level. (C) Enrichment analysis and (D) pathway analysis of the significantly altered 62 DEMs. a, Linoleic acid metabolism; b, Arginine and proline metabolism; c, Caffeine metabolism; d, Cysteine and methionine metabolism; e, Retinol metabolism; f, One carbon pool by folate; g, Alanine, aspartate and glutamate metabolism; h, Lysine degradation; i, Purine metabolism; j, Steroid hormone biosynthesis; k, Glycine, serine and threonine metabolism; l, Tyrosine metabolism. Bioinformatic analysis was performed using OmicStudio tools at https://www.omicstudio.cn/tool and the MetaboAnalyst6.0 online platform.

4. Discussion

The prevalence of HUA is steadily increasing, particularly among younger populations, highlighting the urgent need for enhanced prevention and treatment strategies. XOD inhibitors remain the cornerstone of therapy, effectively lowering serum uric acid levels by targeting XOD activity. While small-molecule inhibitors currently dominate research, bioactive peptides have garnered increasing attention due to their favorable safety profiles and potent efficacy. Numerous studies have reported that peptides derived from animal and plant protein hydrolysates exhibit strong XOD inhibitory activity and effectively reduce uric acid levels *in vivo*[20]. Our previous research demonstrated that peptides derived from *A. davidianus* bone hydrolysate exhibit significant XOD inhibition and nephroprotective effects in hyperuricemic models[10]. However, a comprehensive evaluation of the antihyperuricemic efficacy of ADBP is still lacking. Furthermore, variability in peptide composition and bioactivity among different sources may impact product consistency. While mixed peptide hydrolysates from diverse origins have demonstrated promising bioactive activities, including antihyperuricemic effects, the bioactive monomers responsible for these effects remain largely unidentified. Traditional methods for discovering bioactive peptide monomers are time-consuming and uncertain. Recently, the combination of multi-omics, machine learning, and molecular docking techniques has garnered attention as an efficient approach for screening bioactive peptide monomers[21]. Moreover, multiple peptide monomers may interact with one another, potentially yielding synergistic effects. In addition to exploring the potential peptide monomers, it is essential to establish a standardized peptide hydrolysate to ensure reproducible bioactivity. In this study, we conducted a systematic comparative analysis of nine ADBP samples and developed a reliable HPLC fingerprinting method for quality assessment. Our results identified the ADBP obtained from HNZJJ region as particularly effective in reducing uric acid both *in vitro* and *in vivo*.

A. davidianus bone, a major by-product of *A. davidianus* processing, is rich in Ca, collagen, and minerals. Despite recent advances in processing technologies, studies investigating its functional applications remain limited, hindering the sustainable development of the *A. davidianus* industry. For example, Shanxi Province alone processed approximately 8 000 tons of commercial *A. davidianus* in 2024, much of which resulted in underutilized or discarded bone material[22]. However, emerging research suggests that compounds such as chondroitin sulfate and peptides extracted from *A. davidianus* bone possess antioxidative, anti-inflammatory, and uric acid-lowering properties[23-24]. Our previous work demonstrated that ADBP effectively inhibit XOD and provide nephroprotection[10]. Nonetheless, preliminary trials revealed significant variability in XOD inhibitory activity across ADBP samples from different habitats, with GZQN and HNZJJ sources outperforming others. This variation highlights the influence of habitat on peptide composition and bioactivity. In this study, a comparative analysis of nine ADBP samples confirmed consistently high protein content and a predominance of low-molecular-weight peptides (approximately 99% < 3 kDa), which aligns with prior data from Shanxi Province showing 86% protein content and similar peptide profiles[25]. Mineral content varied significantly among samples, underscoring site-specific differences. Notably, *A. davidianus* bone contains high levels of K, Ca, P, Fe, Zn, and Se, all of which are released during enzymatic hydrolysis. K, Ca, and P synergistically support bone cell function, while Fe, Zn, and Se, nutrients often deficient in Chinese populations[26], play critical physiological roles. Zn and Cu facilitate metallothionein synthesis, aiding heavy metal detoxification, and Se supports vision, immune function, and cancer prevention. The ADBP derived from CQYC region exhibited the highest levels of K, Ca, and P, while all samples contained substantial Se, suggesting the potential of ADBP as a mineral supplement with habitat-dependent variation. Notably, high Se content appears to be a characteristic of peptides derived from *A. davidianus*. Similar studies have shown that the Se content in *A. davidianus* meat exceeds that of nest, ginseng, and soft-shelled turtle[27]. However, few studies have reported similarly high Se content in other amphibians, such as tadpoles, *Necturus maculosus*, and *Bufo bufo*[28-29]. We speculate that this may be partially attributed to the unique habitats and species characteristics of *A. davidianus*. Amino acid profiling was used to assess the peptides' XOD inhibitory potential. The uric acid-lowering activity of peptides correlates with the type, quantity, and position of amino acids, with a higher HAA content generally enhancing XOD inhibition[30]. ADBP from HNZJJ region exhibited the highest levels of HAA ((23.05 ± 0.45) g/100 g), EAA ((19.52 ± 0.39) g/100 g), and TAA ((68.69 ± 1.78) g/100 g), indicating superior inhibitory potential. As known, different origins of ADBP samples may correspond to diverse subspecies of *A. davidianus*, which likely accounts for some of the observed variability in amino acid sequences of proteins and bone collagen types. Additionally, differences in feeding strategies and aquaculture environments among *A. davidianus* farms likely contribute to the variation in ADBP composition. These findings suggest that ADBP from HNZJJ region may represent a promising source of XOD inhibitory peptides from *A. davidianus*. This was confirmed *in vitro*, where the ADBP derived from HNZJJ region demonstrated the strongest XOD inhibition, justifying its selection for further antihyperuricemic evaluation.

Recent efforts have increasingly focused on the development of uric acid-lowering peptides; however, research on quality control in this area remains limited. This study introduces a simple yet robust HPLC fingerprinting method for ADBP sourced from nine distinct habitats, establishing a critical foundation for standardized quality assessment. To our knowledge, this is the first systematic evaluation of the quality of *A. davidianus* bone, marking a significant step toward industry standardization. Similar fingerprinting methods have been successfully applied to other biopeptides derived from corn, *Pseudostellaria heterophylla*, and *Eupolyphaga steleophaga*[31-32]. The adoption of advanced analytical techniques could further enhance ADBP quality evaluation. Hierarchical cluster analysis revealed significant compositional differences among the ADBP samples, with those from HNZJJ region forming a distinct cluster. This variation likely reflects the superior environmental conditions in HNZJJ region, as supported by local surveys[33]. However, cross-regional breeding and transportation complicate the traceability of origin, introducing variability in ADBP quality. Therefore, the development of a comprehensive quality control system for ADBP is essential to ensure consistency and therapeutic reliability.

Current screening methods for uric acid-lowering bioactive substances predominantly rely on *in vitro* XOD inhibition assays and *in vivo* HUA mouse models. While chemical assays provide rapid and reproducible preliminary screening, they lack physiological complexity. In contrast, animal models offer biological relevance

but are hindered by low throughput, high cost, lengthy protocols, interspecies variability, and inconsistent reproducibility, which impede efficient evaluation[34]. To address these challenges, we developed a stable high-uric-acid LO_2 cell model by optimizing induction parameters (600 μg/mL adenosine, 8×10^4 cells/mL density, and a 30-h incubation) based on established protocols[18]. Using this model, ADBP derived from HNZJJ region demonstrated a dose-dependent reduction in uric acid levels, consistent with reports on the efficacy of hesperetin in HUA cell models[35]. Subsequent validation in hyperuricemic mice confirmed that ADBP significantly lowered hepatic uric acid levels by inhibiting both liver and serum XOD and ADA activities. This was coupled with a dose-dependent suppression of hepatic XOD protein expression. Given that elevated uric acid induces oxidative liver damage[36-37], the hepatoprotective effects of ADBP were associated with enhanced antioxidant capacity and improved liver function. These findings align with studies showing that fish bone peptides reduce uric acid levels and mitigate oxidative and inflammatory damage through XOD inhibition[4,38]. Similarly, oral administration of a crude proteolytic digest of shark cartilage has been reported to lower serum uric acid levels in oxonate-induced hyperuricemic rats[39]. Additionally, peptides from other marine fish bones, such as those from Tuna and *Gadus macrocephalus* (*Tilesius*), also exhibited strong XOD inhibitory effects and antihyperuricemic activity[40-41]. The primary mechanism underlying the uric acid-lowering effects is the inhibition of XOD activity. As XOD is a key enzyme in uric acid synthesis, its inhibitors remain prime therapeutic targets. Advanced techniques, including omics, molecular docking, molecular dynamics simulation, and surface plasmon resonance, now facilitate the rapid identification of natural XOD inhibitors[42-43]. Several studies have reported antihyperuricemic peptide monomers derived from marine fish, dairy products, rice, sea cucumbers, and other sources using computer-aided drug discovery methods, demonstrating XOD inhibitory effects, uric acid-lowering activity, and hepatic and renoprotective effects[44]. Although our findings confirm the effective antihyperuricemic action and XOD inhibition of ADBP, the specific bioactive peptide monomers remain unidentified. Future research aimed at isolating and characterizing these peptides is crucial to fully understanding their therapeutic potential. In conclusion, ADBP derived from HNZJJ region effectively alleviates HUA and its associated sequelae by inhibiting uric acid biosynthesis and enhancing antioxidant defenses, underscoring its promise for clinical and commercial development.

Additionally, untargeted metabolomics analysis of liver tissues from HUA mice was performed to explore the metabolic pathways potentially responsible for the antihyperuricemic and hepatoprotective effects of ADBP. HUA is commonly associated with metabolic disturbances, particularly in the metabolism of amino acids, nucleotides, lipids, and carbohydrates[45]. In the present study, ADBP treatment positively influenced liver metabolism in HUA mice, as evidenced by the relatively shorter distance between the ADBP group and the control group in the PCA plot, compared to the model group. This suggests that the liver metabolite composition in the ADBP group was more similar to that of the control group than to the model group. Further analysis revealed that a total of 62 DEMs in the ADBP group were restored to levels closer to those of the control group, as compared to the model group.

A total of 5 KEGG enrichment pathways, including linoleic acid metabolism, arginine and proline metabolism, caffeine metabolism, cysteine and methionine metabolism, and purine metabolism, were strongly associated with these phenotype-related metabolites. These pathways are likely key contributors to the ameliorative effects of ADBP in HUA mice.

Lipid metabolism, including linoleic acid metabolism, is often disrupted in patients with HUA[46]. In this study, the metabolites 12,13-EpOME and 9,10-DiHOME in linoleic acid metabolism were restored to levels closer to those of the control group in the ADBP-treated mice compared to the model group. Additionally, other downregulated lipids, such as FAHFA (8:0/10:0), FFA (12:1), FFA (18:4), pinolenic acid, lysophosphatidylcholine (LPC, 12:0/0:0), 5 types of lysophosphatidylethanolamine (LPE), phosphatidylethanolamine lyso alkenyl 18:2, carnitine $C_{10:1}$, and carnitine $C_{18:3}$, were reversed by ADBP intervention in the liver of HUA mice. These altered lipid metabolites were predominantly associated with uric acid metabolism, oxidative stress, and inflammation. Interestingly, carnitine deficiency has been shown to cause lactate accumulation, which in turn inhibits uric acid excretion[47]. In this study, the increased levels of carnitine in the liver of ADBP-treated mice suggest a potential promotion of uric acid excretion by ADBP. Moreover, abnormal levels of LPC and LPE can contribute to lipid peroxidation and oxidative stress[48]. ADBP treatment effectively modulated the levels of LPC and LPE in HUA mice, potentially mitigating oxidative damage. In line with our findings, Qin et al.[49] confirmed that HUA is accompanied by metabolic disturbances, particularly in lipid and amino acid metabolism. HUA also triggers oxidative and inflammatory damage, leading to reduced antioxidant enzyme activity and increased secretion of inflammatory cytokines, which in turn disrupt metabolic pathways such as linoleic acid metabolism, glycerophospholipid metabolism, sphingolipid metabolism, and arachidonic acid metabolism. ADBP may alleviate these disruptions by reducing reactive oxygen species (ROS) levels during excessive hepatic uric acid biosynthesis, as evidenced by the increased liver antioxidant activity in response to ADBP treatment, indirectly attenuating HUA-induced lipid metabolism disorders. These results suggest that lipid metabolism is severely disturbed in HUA mice, and ADBP treatment alleviates HUA-induced lipid metabolism disorders. Amino acid metabolism also plays a crucial role in mitigating HUA. Our analysis identified 15 amino acids and their derivatives from a set of 62 candidate DEMs in HUA mice that were notably restored by ADBP treatment. These metabolites were enriched in several amino acid metabolism pathways, including arginine and proline metabolism, as well as cysteine and methionine metabolism. Consistent with our findings, Liu et al.[50] reported that dietary probiotics improved HUA-induced metabolic disorders, such as those related to arginine and proline metabolism, linoleic acid metabolism, and purine metabolism. Notably, arginine and proline are strongly associated with inhibiting kidney oxidative damage in HUA[51]. Certain amino acids, such as arginine, glycine, and glutamine, serve as precursors in uric acid biosynthesis, making amino acid homeostasis essential in HUA. Similar studies have shown that significant alterations in arginine metabolism occur in both HUA and gout patients, with arginine anabolic metabolism contributing to oxidative stress and inflammation[52]. Additionally,

the caffeine metabolism pathway was significantly enriched in the ADBP-treated group. Correspondingly, the elevated levels of 3-methylxanthine and 7-methylxanthine in the model group were significantly reduced following ADBP treatment. These findings align with those of Yang et al.[53], who demonstrated that the anti-HUA effects of taurine could be achieved through modulation of caffeine metabolism, phenylalanine metabolism, nicotinate and nicotinamide metabolism, and retinol metabolism. Caffeine, as an adenosine receptor antagonist, suppresses adenosine activity by competing for binding to its receptor[54]. We hypothesize that ADBP plays a crucial role in alleviating liver uric acid biosynthesis and oxidative stress, potentially through the modulation of caffeine metabolism. Purine metabolism disorders are a hallmark of HUA, characterized by varying trends in purine forms, including purine nucleotides, nucleosides, and bases[55]. In this study, 11 purine nucleotides and their metabolites (6 upregulated and 5 downregulated) were disrupted in the model group compared to the control group, indicating dysfunction in liver purine metabolism induced by HUA. These disturbances may, at least in part, contribute to the elevated uric acid levels observed in HUA mice. However, ADBP intervention restored these altered DEMs to levels closer to those of the control group, suggesting that ADBP alleviates purine metabolism disorders. The accumulation of ROS is positively correlated with excessive uric acid biosynthesis and disruption of purine metabolism, which in turn triggers oxidative stress and inflammation[10,56]. The improvement in liver antioxidant capacity in the ADBP-treated group supports the hypothesis that ADBP enhances purine metabolism. This is evidenced by the increased antioxidant indices (SOD, CAT, GSH) and reduced MDA content in the liver of HUA mice. In reality, the metabolic disorders induced by HUA are not the result of a single factor, but rather the outcome of a "vicious cycle network". HUA is both a cause and an effect, amplifying this network. Uric acid interferes with normal metabolic homeostasis through multiple mechanisms, including inflammation, oxidation, and gut microbiota imbalance, thereby influencing its biosynthesis and excretion and triggering systemic metabolic disorders[57]. In this study, ADBP treatment effectively suppressed excessive liver uric acid biosynthesis and promoted liver antioxidant activity, significantly alleviating HUA-induced metabolic disturbances. Taken together, these findings demonstrate that ADBP exerts antihyperuricemic and hepatoprotective effects through multiple metabolic pathways.

5. Conclusion

This study systematically compared ADBP samples from nine habitats and developed a reliable HPLC fingerprinting method for quality control. ADBP derived from HNZJJ region demonstrated potent uric acid-lowering activity in a high-uric-acid LO_2 cell model, effectively inhibiting hepatic uric acid synthesis while enhancing antioxidant capacity and liver function in hyperuricemic mice. Metabolomic analysis revealed that the beneficial effects of ADBP in alleviating HUA may be attributed to the repair of liver metabolic disorders and the improvement of oxidative stress. These findings provide comprehensive compositional and functional insights, supporting the commercial development of ADBP. However, further research is required to isolate the active antihyperuricemic peptides and assess the storage stability of ADBP. In conclusion, our results underscore ADBP's potential as a safe and effective dietary supplement for the prevention and management of HUA.

Conflict of interest

Xinhui Xing is an editorial board member for *Food Science and Human Wellness* and was not involved in the editorial review or the decision to publish this article. The authors report there are no competing interests to declare.

Acknowledgements

This study was financially supported by the Shenzhen Science and Technology Program (JCYJ20240813112052067), the Haday Visionary Science Advancement Fund.

Appendix A. Supplementary data

Supplementary data associated with this article can be found, in the online version, at http://doi.org/10.26599/FSHW.2025.9250796.

References

[1] P.K. Im, C. Kartsonaki, M.G. Kakkoura, et, al., Hyperuricemia, gout and the associated comorbidities in China: findings from a prospective study of 0.5 million adults, Lancet Reg. Health West. Pac. 58 (2025) 101572. https://doi.org./10.1016/j.lanwpc.2025.101572.

[2] Z. Sun, K. Wu, I. Ullah, et al., Recent advances in xanthine oxidase inhibitors, Mini-rev. Med. Chem. 24 (2024) 1177-1186. https://doi.org./10.2174/1389557523666230913091558.

[3] Z. Xu, M. Gan, W. Guan, et al., *In slico* screening and *in vitro* identification of hyperuricemia-inhibiting peptides from *Trachurus japonicus*, Foods 14 (2025) 524. https://doi.org./10.3390/foods14030524.

[4] W. Meng, J. Zhang, H. Hou, et al., Exploring the structures and molecular mechanisms of bioactive compounds from marine foods for hyperuricemia prevention: a systematic review, Crit. Rev. Food. Sci. Nutr. (2025) 1-19. https://doi.org./10.1080/10408398.2025.2464700.

[5] J. Zhan, Q. Zhang, S. Mei, et al., Study on antioxidant synergistic anti-inflammatory peptide from giant salamander (*Andrias davidianus*): functional mechanism and delivery by nano-starch, Food Sci. Hum. Wellness (2025) https://doi.org./10.26599/FSHW.2025.9250512.

[6] L. Shu, M. Yang, N. Liu, et al., Short hexapeptide optimized from rice-derived peptide 1 shows promising anti-hyperuricemia activities, J. Agric. Food. Chem. 70 (2022) 6679-6687. https://doi.org./10.1021/acs.jafc.2c00354.

[7] X.L. Luo, T. Liu, F.Q. Feng, et al., Recent progress in research on hyperuricemia and uric acid-lowering peptides. Food Sci. 42 (2021) 340-348. https://doi.org./10.7506/spkx1002-6630-20200221-232.

[8] C. Guan, Z. Tan, S. Li, et al., Transcriptomic analysis of *Andrias davidianus* meat and experimental validation for exploring its bioactive components as functional foods, Food Sci. Hum. Wellness 13 (2024) 166-172. https://doi.org./10.26599/FSHW.2022.9250014.

[9] J. Wang, Y. Liu, H. Guo et al., Cultured Chinese giant salamander skin and skin secretions as a source of bioactive peptides for food and medicine, Food Sci. Anim. Resour. 45 (2025) 109-125. https://doi.org./10.5851/kosfa.2024.e114.

[10] W. Li, H. Chen, H. Chen et al., *Andrias davidianus* bone peptides alleviates hyperuricemia-induced kidney damage *in vitro* and *in vivo*, Food Sci. Hum. Wellness 13 (2024) 1886-1905. https://doi.org./10.26599/FSHW.2022.9250157.

[11] S. Li, C. Guan, Y. Wang, et al., Screening of Chinese giant salamander meat hydrolysates with DPP-IV inhibitory activity and systematic elucidation of their hypoglycemic functions in mouse model, Food Sci. Hum. Wellness (2025) https://doi.org./10.26599/FSHW.2024.9250206.

[12] D. He, W. Zhu, W. Zeng, et al., Nutritional and medicinal characteristics of Chinese giant salamander (*Andrias davidianus*) for applications in healthcare industry by artificial cultivation: a review, Food Sci. Hum. Wellness 7 (2018) 1-10. https://doi.org./10.1016/j.fshw.2018.03.001.

[13] E. Noviana, G. Indrayanto, A. Rohman, Advances in fingerprint analysis for standardization and quality control of herbal medicines, Front. Pharmacol. 13 (2022) 853023. https://doi.org./10.3389/fphar.2022.853023.

[14] J. Wang, D. Luo, M. Liang, et al., Spectrum-effect relationships between high-performance liquid chromatography (HPLC) fingerprints and the antioxidant and anti-inflammatory activities of collagen peptides, Molecules 23 (2018) 3257. https://doi.org./10.3390/molecules23123257.

[15] C. Wang, H. He, J. Zhang, et al., High performance liquid chromatography (HPLC) fingerprints and primary structure identification of corn peptides by HPLC-diode array detection and HPLC-electrospray ionization tandem mass spectrometry, J. Food Drug Anal. 24 (2016) 95-104. https://doi.org./10.1016/j.jfda.2015.05.005.

[16] W. Li, X. Zhang, R. Chen et al., HPLC fingerprint analysis of *Phyllanthus emblica* ethanol extract and their antioxidant and anti-inflammatory properties, J. Ethnopharmacol. 254 (2020) 112740. https://doi.org./10.1016/j.jep.2020.112740.

[17] Z. Wang, Y. Han, L. Zhang et al., The utilization of a data fusion approach to investigate fingerprint profiles of dark tea from China's different altitudes, Food Chem.: X 22 (2024) 101447. https://doi.org./10.1016/j.fochx.2024.101447.

[18] D. Liu, J. Ren, M. Liang, Establishment of the cell model of hyperuricemia and its application in screening food-derived anti-hyperuricemic peptides, Mod. Food Sci. Technol. 33 (2017) 72-79. https://doi.org./10.13982/j.mfst.1673-9078.2017.8.012.

[19] L. Hao, Y. Ding, Y. Fan, et al., Identification of hyperuricemia alleviating peptides from Yellow Tuna *Thunnus albacares*, J. Agric. Food. Chem. 21 (2024) 12083-12099. https://doi.org./10.1021/acs.jafc.3c09901.

[20] S. Feng, S. Wu, F. Xie, et al., Natural compounds lower uric acid levels and hyperuricemia: Molecular mechanisms and prospective, Trends Food Sci. Technol. 123 (2022) 87-102. https://doi.org./10.1016/j.tifs.2022.03.002.

[21] J. Chang, H. Wang, W. Su, et al., Artificial intelligence in food bioactive peptides screening: Recent advances and future prospects, Trends Food Sci. Technol. 156 (2025) 104845. https://doi.org/10.1016/j.tifs.2024.104845.

[22] X. Sun, Z. Zhang, Z. Liu, et al., Research report on the development of fishery industry and fishery insurance in Shaanxi Province, Insur. Theory Pract. 95(5) (2024) 81-92.

[23] W. Zhu, Y. Ji, Y. Wang, et al., Structural characterization and *in vitro* antioxidant activities of chondroitin sulfate purified from *Andrias davidianus* cartilage, Carbohydr. Polym. 196 (2018) 398-404. https://doi.org./10.1016/j.carbpol.2018.05.047.

[24] Y. Wang, X. Hong, Q. Jin, et al., Review of Chinese giant salamander bone collagen peptides, Farm Products Processing (2024) 73-77,84. https://doi.org./10.16693/j.cnki.1671-9646(X).2024.23.015.

[25] X. Zheng, D. Chen, W. Su, et al., Effect of bone peptide of giant salamander on alleviating hyperuric acid in mice, Food Ferment. Ind. 51 (2025) 267-275. https://doi.org./10.13995/j.cnki.11-1802/ts.038766.

[26] S. Liu, A. Yang, G. Peng, et al., Determination and analysis of several important mineral in cartilage and muscle of feeding China giant salamander using ICP-AES, Sci. Technol. Food Ind. (2007) 225-226. https://doi.org./10.3969/j.issn.1002-0306.2007.08.070.

[27] M. Wang, Q. Luo, H. Wang, et al., Determination and evaluation of mineral elements in muscle of giant salamander Zhangjiajie, Jiangsu Agricultural Sciences 5 (2014) 238-239. https://doi.org./10.15889/j.issn.1002-1302.2014.05.027.

[28] C. M. Lanctôt, T. Cresswell, P.D. Callaghan, et al., Bioaccumulation and biodistribution of selenium in metamorphosing tadpoles, Environ. Sci. Technol. 51 (2017) 5764-5773. https://doi.org/10.1021/acs.est.7b00300.

[29] K. Dobrovoljc, I. Falnoga, M.T. Žnidarič, et al., Cd, Cu, Zn, Se, and metallothioneins in two amphibians, *Necturus maculosus* (Amphibia, Caudata) and *Bufo bufo* (Amphibia, Anura), Biol. Trace Elem. Res. 150 (2012) 178-194. https://doi.org/10.1007/s12011-012-9461-2.

[30] Z. Yuan, S. Cheng, D. Wu, et al., Advances in research on xanthine oxidase inhibitory peptides, Food Sci. 43 (2022) 355-363. https://doi.org./10.7506/spkx1002-6630-20210604-058.

[31] X. Lai, H. Song, G. Yan, et al., Fingerprint profile analysis of *Eupolyphaga steleophaga* polypeptide based on UHPLC-MS and its application, Pharmaceuticals 18 (2025) 166. https://doi.org./10.3390/ph18020166.

[32] L. Zhao, H. Yang, C. Jiang, et al., Studies on the oral absorption of cyclic peptides from *Pseudostellaria heterophylla* and interacting with membrane receptors, Fitoterapia 156 (2022) 105072. https://doi.org./105072. 10.1016/j.fitote.2021.105072.

[33] F. Gao, J. Xiang, Y. Xie, et al., Habitat quality assessment of the Chinese giant salamander (*Andrias davidianus*) in Zhangjiajie based on community diversity of macroinvertebrates, Freshwater Fisheries 53 (2023) 102-112. https://doi.org./10.3969/j.issn.1000-6907.2023.01.013.

[34] C. Hou, W. Sha, Z. Xu et al., Culture and establishment of self-renewing human liver 3D organoids with high uric acid for screening antihyperuricemic functional compounds, Food Chem. 374 (2022) 131634. https://doi.org./10.1016/j.foodchem.2021.131634.

[35] M. An, C. Shen, S. Zhang, et al., Anti-hyperuricemia effect of hesperetin is mediated by inhibiting the activity of xanthine oxidase and promoting excretion of uric acid, Front. Pharmacol. 14 (2023) 1128699. https://doi.org./10.3389/fphar.2023.1128699.

[36] Y. Mao, H. Xu, P. Xia, *Ilex cornuta* leaves extracts ameliorate hyperuricemia by modulating uric acid transporters, J. Ethnopharmacol. 336 (2025) 118618. https://doi.org./10.1016/j.jep.2024.118618.

[37] M. Gherghina, I. Peride, M. Tiglis, et al., Uric acid and oxidative stress—relationship with cardiovascular, metabolic, and renal impairment, Int. J. Mol. Sci. 23 (2022) 3188. https://doi.org./10.3390/ijms23063188.

[38] C. Wu, Q. Hu, X. Peng, et al., Marine fish protein peptide regulating potassium oxonate-induced intestinal dysfunction in hyperuricemia rats helps alleviate kidney inflammation, J. Agric. Food. Chem. 71 (2022) 320-330. https://doi.org./10.1021/acs.jafc.2c04017.

[39] I. Murota, T. Tamai, T. Baba, et al., Uric acid lowering effect by ingestion of proteolytic digest of shark cartilage and its basic fraction, J. Food Biochem. 34 (2010) 182-194. https://doi.org./10.1111/j.1745-4514.2009.00273.x.

[40] Q. Zhao, Y. Meng, J. Liu, et al., Separation, identification and docking analysis of xanthine oxida,se inhibitory peptides from pacific cod bone-flesh mixture, LWT-Food Sci. Technol. 167 (2022) 113862. https://doi.org/10.1016/j.lwt.2022.113862.

[41] Z. Yu, R. Kan, S. Wu, et al., Xanthine oxidase inhibitory peptides derived from tuna protein: virtual screening, inhibitory activity, and molecular mechanisms, J. Sci. Food. Agric. 101 (2021) 1349-1354. https://doi.org./10.1002/jsfa.10745.

[42] H. Liu, R. Xie, Q. Dai, et al., Exploring the mechanism underlying hyperuricemia using comprehensive research on multi-omics, Sci. Rep. 13 (2023) 7161. https://doi.org./10.1038/s41598-023-34426-y.

[43] Y. Wang, Z. Yu, Z. Zhang, et al., Integrating metabolomics with network pharmacology to reveal the mechanism of *Poria cocos* in hyperuricemia treatment, J. Ethnopharmacol. 337 (2025) 118977. https://doi.org./10.1016/j.jep.2024.118977.

[44] Y. Chen, H. Li, Y. Cai, et al., Anti-hyperuricemia bioactive peptides: a review on obtaining, activity, and mechanism of action, Food Funct. 15 (2024) 5714-5736. https://doi.org./10.1039/d4fo00760c.

[45] R. Chen, Q. Wang, Z. Li, et al., Studies on effect of Tongfengxiaofang in HUM model mice using a UPLC-ESI-Q-TOF/MS metabolomic approach, Biomed. Chromatogr. 35 (2021) 5118. https://doi.org./10.1002/bmc.5118.

[46] Y. Chen, C. Pei, Y. Chen, et al., Kidney tea ameliorates hyperuricemia in mice *via* altering gut microbiota and restoring metabolic profile, Chem. Biol. Interact. 376 (2023) 110449. https://doi.org./10.1016/j.cbi.2023.110449.

[47] Y. Wang, M. Zhao, Y. Xin, et al., ^{1}H-NMR and MS based metabolomics study of the therapeutic effect of cortex fraxini on hyperuricemic rats, J. Ethnopharmacol. 185 (2016) 272-281. https://doi.org./10.1016/j.jep.2016.03.043.

[48] B. Shan, T. Chen, B. Huang, et al., Untargeted metabolomics reveal the therapeutic effects of Ermiao wan categorized formulas on rats with hyperuricemia, J. Ethnopharmacol. 281 (2021) 114545. https://doi.org./10.1016/j.jep.2021.114545.

[49] N. Qin, M. Qin, W. Shi, et al., Investigation of pathogenesis of hyperuricemia based on untargeted and targeted metabolomics, Sci. Rep. 12 (2022) 13980. https://doi.org./10.1038/s41598-022-18361-y.

[50] P. Liu, P. Hu, M. Jin, et al., Compound probiotics alleviate hyperuricemia-induced renal injury *via* restoring gut microbiota and metabolism, BMC Microbiol. 25 (2025) 280. https://doi.org./10.1186/s12866-025-04012-5.

[51] H. Li, S. Li, H. Yang, et al., l-Proline alleviates kidney injury caused by AFB1 and AFM1 through regulating excessive apoptosis of kidney cells, Toxins 11 (2019) 226. https://doi.org./10.3390/toxins11040226.

[52] X. Wu, C. You, The biomarkers discovery of hyperuricemia and gout: proteomics and metabolomics, Peer J 11 (2022) e14554. https://doi.org./10.7717/peerj.14554.

[53] X. Yang, H. Li, D. Qumu, et al., Taurine alleviates hyperuricemia-induced nephropathy in rats: insights from microbiome and metabolomics, Front. Nutr. 12 (2025) 1587198. https://doi.org./10.3389/fnut.2025.1587198.

[54] A.K. Mandal, T.R. Merriman, H. K. Choi, et al., Caffeine inhibits both basal and insulin-activated urate transport, Arthritis Rheumatol. 76 (2024) 1658-1669. https://doi.org./10.1002/art.42940.

[55] A. James, H. Ke, T. Yao, et al., The role of probiotics in purine metabolism, hyperuricemia and gout: Mechanisms and interventions, Food Rev. Int. (2021) 1-17. https://doi.org./10.1080/87559129.2021.1904412.

[56] R. Tian, C. Yang, S. Chai, et al., Evolutionary impacts of purine metabolism genes on mammalian oxidative stress adaptation, Zool. Res. 43 (2022) 241. https://doi.org./10.24272/j.issn.2095-8137.2021.420.

[57] A.N.C. Simão, M. A.B. Lozovoy, I. Dichi, The uric acid metabolism pathway as a therapeutic target in hyperuricemia related to metabolic syndrome, Expert Opin. Ther. Targets. 16 (2012) 1175-1187. https://doi.org/10.1517/14728222.2012.723694.